Passive Thermochemical Energy Storage System for Low Power Sensor Modules for Space Applications

by

Salil Rajendra Rabade

A Thesis Presented in Partial Fulfillment
of the Requirements for the Degree
Master of Science

Approved November 2016 by the
Graduate Supervisory Committee:

Jekan Thanga, Co–Chair
Huei Ping Huang, Co-Chair
Konrad Rykaczweksi

ARIZONA STATE UNIVERSITY

December 2016

ABSTRACT

Surface exploration of the Moon and Asteroids can provide important information to scientists regarding the origins of the solar-system and life . Small robots and sensor modules can enable low-cost surface exploration. In the near future, they are the main machines providing these answers. Advanced in electronics, sensors and actuators enable ever smaller platforms, with compromising functionality. However similar advances haven't taken place for power supplies and thermal control system. The lunar south pole has temperatures in the range of -100 to -150 ^{o}C. Similarly, asteroid surfaces can encounter temperatures of -150 ^{o}C. Most electronics and batteries do not work below -40 ^{o}C. An effective thermal control system is critical towards making small robots and sensors module for extreme environments feasible.

In this work, the feasibility of using thermochemical storage materials as a possible thermal control solution is analyzed for small robots and sensor modules for lunar and asteroid surface environments. The presented technology will focus on using resources that is readily generated as waste product aboard a spacecraft or is available off-world through In-Situ Resource Utilization (ISRU).

In this work, a sensor module for extreme environment has been designed and prototyped. Our intention is to have a network of tens or hundreds of sensor modules that can communicate and interact with each other while also gathering science data. The design contains environmental sensors like temperature sensors and IMU (containing accelerometer, gyro and magnetometer) to gather data. The sensor module would nominally contain an electrical heater and insulation. The thermal heating effect

provided by this active heater is compared with the proposed technology that utilizes thermochemical storage chemicals.

Our results show that a thermochemical storage-based thermal control system is feasible for use in extreme temperatures. A performance increase of 80% is predicted for the sensor modules on the asteroid Eros using thermochemical based storage system. At laboratory level, a performance increase of 8 to 9 % is observed at ambient temperatures of -32^{o}C and -40 ^{o}C.

To my parents Dr. Rajendra Rabade, Dr. Vijaya Rabade

and my Uncle Dr. Tejas Dhadphale

ACKNOWLEDGMENTS

Firstly, I want to express gratitude to my Chair and Mentor Dr. Jekan Thanga for his guidance, support and motivation. His constant encouragement has helped me explore a facet of engineering I wouldn't have explored otherwise. This has helped me grow as an engineer and as a person.

I would like to thank my Dr Huei Ping Huang and Dr. Konrad Rykaczweksi who have agreed to be on my committee and provided me with the right information at the right time.

I would like to thank my colleagues and friends at SpaceTREx, Lab. I would like to specially thank Laksh Raura , Andrew Warren and Aman Chandra for their valuable inputs. Lastly, I want to thank all my friends and folks who have been a major part of my journey at ASU and who motivated me throughout my research.

TABLE OF CONTENTS

Page

CHAPTER Page

LIST OF TABLES

Table Page

LIST OF FIGURES

Figure Page

Figure Page

Figure Page

CHAPTER 1

INTRODUCTION

1.1 Background

Exploration of the planets and moons on the solar system started with flyby spacecraft, followed by orbiters, landers and rovers. Flyby spacecraft and orbiters are increasing in capability, offering high resolution imagers, but they are often in-adequate to answer questions about the formation of geological features of a surface. Landers and rovers provide detailed in-situ data of a planet or moon's surfaces that cannot be replaced by orbital or flyby imagery.

For example, the images and science data from the Mars curiosity rover has contributed to answering the geological surface features of Mars. However, the mobility of one vehicle is limited and as such restricts its exploration range and capabilities. Moreover, the science mission is completely dependent on one robot. Multiple robots can increase the exploration range and number data points but this can get expensive. Additionally, asteroids and comets, hold tantalizing mysterious that can answer fundamental questions regarding the origin of the solar-system, life and formation of planetary bodies.

These small bodies have gravity in range of 10^{-4} to 10^{-6} m/s^2 . This makes it very difficult to have such a terrestrial exploration vehicle.

Figure 1-Philae lander robot [1]

The Philae lander was a robotic lander deployed by the ESA along with the Rosetta mission. Although Philae had partial success in landing on Comet 67P/ Churyumov–Gerasimenko, it was after two failed attempts that caused it to bounce of the surface. The final landing site was unplanned and as a consequence the lander received less than expected sunlight, thus reducing the duration of the science mission. It is hence very risky to have a science mission without any redundancy on extreme environments such as the surface of comets and asteroids.

A better option would be to deploy multiple small robots or wireless sensor modules to achieve the science mission objectives. The Hedgehog robot is a system that is currently being developed by Stanford and NASA JPL to explore the surface of Phobos and has the above objective in mind [2]. The main drawback with this methodology is the lack of knowledge of asteroid and comet surface properties. Without this information it is difficult to know the mobility limitations imposed on the robot.

A constellation of small low-mass sensor modules is an attractive option. These modules are stationary and can communicate with each other using Radio Frequency. The advantage is that these systems are relatively, simple, low-cost and low-mass. They

will also have a lower power consumption as they are stationary. By having different sensors on each node of the network complex science experiments could be done. Since, the sensor module network would cover a larger area, the collected data would provide a better understanding about the surface or geology of the body. One of the main challenges is limited energy storage. A second major challenge is thermal management of the module, to ensure the system can maintain a minimum storage and operating temperature.

The high energy needs of a sensor module can be fulfilled using high efficiency PEM fuel-cells that operate at 65 % efficiency. PEM fuel cell have the potential to have high energy density, much higher than batteries. A concept developed by Strawser, Thangavelautham and Dubowsky, 2014 can have an energy density of 2,000 Wh/kg

The output from a fuel cell is electricity, heat and water. Typically, solar photovoltaics are used to charge a rechargeable battery to provide electrical energy.

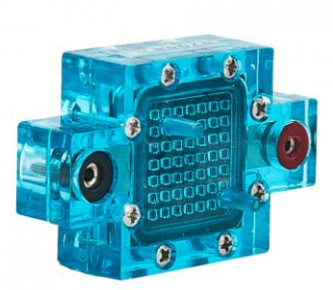

Figure 2- PEM Fuel cell [3]

With the right system design, Fuel cells (Figure 2) can fulfill the power needs under extreme temperature conditions. If sensor modules operate in deep space, due to lack of solar energy, they will face a major thermal challenge of keeping warm.

A robust thermal control mechanism is needed to ensure the successful completion of any science mission. Typical space systems rely on solar energy and waste heat from electronics to survive the freezing temperatures. When this is not possible, they rely on radioactive materials that decay and produce heat. Passive mechanisms do not rely on electronics to control heat, while active control systems rely on electronics to control heat. Passive systems are typically simple and robust, but have reduced efficiency over active systems.

1.2 Problem Statement

Thermal control presents a big challenge. Active heaters are needed if the sensor modules are to function on planetary bodies that are shrouded in darkness and there is very little incident sunlight. As there is little incident sunlight, active thermal control can maximize efficiency. However if are to explore bodies in the inner solar system, there is plenty of sunlight and ambient temperature can be sufficiently high during most times of the day. A passive heat generation system is overall simple and robust and is the preferred solution when developing sensor modules that are going to be deployed by the tens or hundreds. Complex electronics poses numerous concerns, as they are one more system that can fail due to temperature and radiation and hence a simple, elegant system that exploits physics to operate has important applications for space systems applications.

Thermochemical Energy Storage Systems (TCESS) have been widely used for solar energy storage. TCESS are passive systems that exploit sorption and hydration exothermic reactions. The reactants are water (sorbate) and a suitable chemical (sorbent).

The design and development process is done taking into account the crucial thermal control challenges faced in space systems. These are:

1. Passive heating system

It is desireable to have passive thermal control systems that can generate heat using stored chemical energy. It must meet the mass and volume constraints of a space system.

2. Utilizing Non -Radioactive elements

It is desireable to have non- radioactive components aboard spacecraft to simplify launch and safety assurance.

1.3 Scope

The focus of the thesis is to study feasibility of low mass TCESS for sensor network modules. The sensor module uses off-the-shelf electronic and the selection criteria included low-power consumption. The trade study focuses on choosing the optimal chemical for the heating application from the literature survey. The preliminary experiments are not done in a vacuum and hence the exact effect of a space environment is not replicated. Chemicals that are readily available in the market are used. The experiments and validation work focuses on:

- Response of the sorbent when different quantities of water are used.
- Comparison of the sensor module temperatures profile using TCESS as a thermal control system, using Kapton heaters and when no thermal control is present.

1.4 Objectives

The objective of the thesis is analyze the feasibility of thermochemicals for heating sensor modules in space and off-world environments. Sensor modules placed on

an off-world surface will undergo day-night cycles that result in extreme temperature fluctuations. An effective thermal control system will capture heat during day time and save it for heating up the sensor module during the cold night time. The sensor modules have been designed to maximize their thermal insulation properties and this has involved selecting an optimal geometry. The variation of performance in space and on earth is predicted using the thermal model. A trade study has been performed to identify and test candidate thermochemicals for maximizing heating performance in the night time .

CHAPTER 2

LITERATURE REVIEW

Thermal control has been of critical interest to the space community ever since the start of the space age in 1957. Maintaining operating temperatures was critical for the survival of robots and humans alike in a hostile environment. One of the main lessons learned from the moon landing was overheating of batteries and other components due to collection of moon dust. The lack of convection in space means that the time taken to cool down is longer as radiation is slower heat transfer phenomena than convection. Currently, astronauts face a similar heating problem during extra vehicular activity from the international space station. Astronauts wear a liquid cooling and ventilation garment to provide necessary cooling effect. As these missions are in earth orbit, overheating is the primary concern. In deep space though, the primary concern is overcooling. Similar advances in heating technology haven't taken place as RTG's and conventional heating mechanisms are sufficient to provide heat to space crafts. RTG's are used to provide both power and heat to the spacecraft. RTG's are not a feasible solution for small sensor modules as they are expensive, pose security concerns and are radioactive. Small sensor modules benefit from non-radioactive sources for heat generation/storage in deep space.

2.1 Sensor Modules

Sensor modules are generally defined as small devices that may house multiple sensors used to collect scientific data. These sensors if deployed by the tens or hundreds can collect valuable data over a larger area. Low power sensors such as Intel's grenade sensor with the ability to detect levels of nitrogen, oxygen and carbon monoxide have

been used by fireman in case of emergency and dangerous fires. Most sensor modules have been developed for short term use in mind. Typically, the power requirements cannot be met for long term use. For long term usage, fuel cells and alternatives to batteries are a viable alternative. Wireless Sensor networks have so far focused on communication aspect of the sensor networks. Minimizing the power consumption has always been the main goal of this research.

Figure 3- Intel Sensor Module[4]

A sensor module was designed for off-world application at MIT's Field and Space Robotics Laboratory with the main goal of achieving a robust passive thermal design and exploring the feasibility of fuel cells as a long duration power supply. This sensor module tested the feasibility of fuel cells for terrestrial and space applications. The design was based on that of a thermos wherein a vacuum is created between the inner and outer spheres. The research also focused on PEM fuel cell analysis although no in situ experiment was carried out. The loss of vacuum meant the experiment did not give the expected temperature profile. The sensor module was tested in environments of 249 K and reached steady state temperature within 4-6 hours [5].

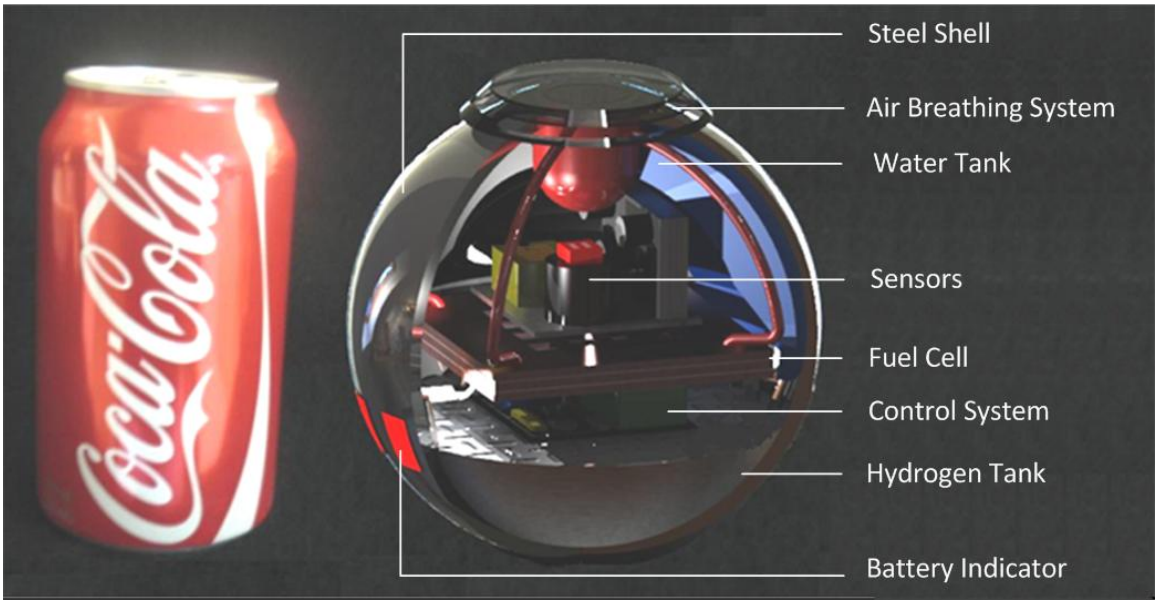

Figure 4- MIT FSRL's proposed sensor module. [5]

2.2 Power System

Proton Electron Membrane (PEM) fuel cells can be used to provide long duration power . Fuel cells take in hydrogen and oxygen as input and provide water, heat and electricity as output. The reaction is exothermic and hence heat is released in the process. Lithium ion batteries have traditionally specific energy density in the range of 120Wh/kg. Lithium hydride powered fuel cells can have storage densities from 3800 Wh/kg to 4900 Wh/kg utilizing ambient air. [6]

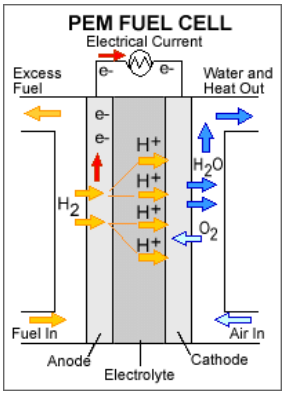

Figure 5- Working of a Fuel cell. [7]

A passive lithium hydride generator has been developed for this purpose and can last upto 60 days. The passive lithium hydride generator works as a source of hydrogen for the fuel cell. The work done here shows the passive generator working for more than 60 days at atmospheric conditions. Lithium hydride forms lithium hydroxide as a byproduct and that can affect the overall system performance [6]. Fuel cells also face operating temperature limitations

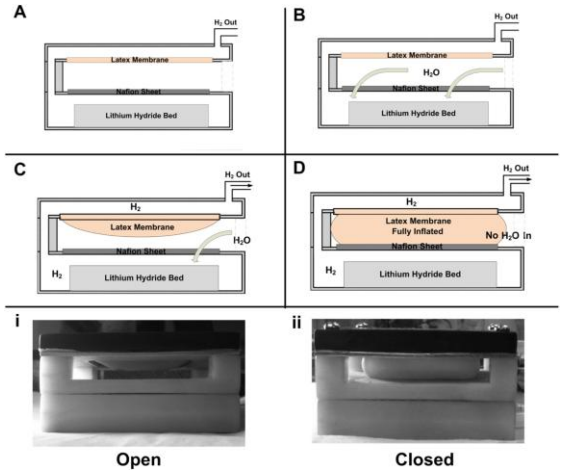

Figure 6- Passive Lithium Hydride Generator. [6]

Fuel cells normally need to operate in the 353K and above range. Fuel cells operating at sub zero conditions have been tested but face certain restrictions. The restriction being operation carried out at lower current densities to avoid higher water generation rates that can cause freezing of the water. This is the main system requirement. Morin et al studied water management issues in a PEM fuel cell at subzero temperatures using Small Angle Neutron scattering (SANS) and Electrochemical Impedance Spectroscopy techniques (EIS). They operated the fuel cell at -4^0C with a voltage of 0.8V and current density of 40 mA/cm^2. As this is an exothermic reaction a 3

^{0}C rise was reported [8]. This shows that by adjusting the voltage and current densities, it is possible to operate fuel cells at low temperatures.

2.3 Thermal System

The thermal design of a sensor module used on off-world surfaces depends entirely on the thermal environment. The thermal environment depends on the solar load on the planet, the albedo of the planet and the irradiance from the planet surface. The main goal of a thermal control system is to ensure all the subsystems in their operational temperature range. Thermal control mechanisms are generally divided into two: [9,10]

2.3.1 Passive control

Passive Control- Passive thermal systems are those that don't use electrical systems to produce heat or a cooling effect. Passive systems primarily focus on controlling the rate of heat flow. They include

1. Surface Finishes – Surface finishes can increase or decrease the absorbed heat based on their optical properties like emissivity and absorptivity. Aluminum coatings can be used to reduce absorption of solar energy while black paints can increase the absorption of energy. Generally black paints are used internally to increase surface to surface heat transfer between the internal surfaces. Surface finishes degrade at high temperatures. White paints tend to show an increase in absorptivity of energy while black paints demonstrate a decrease of absorptivity of energy .[10]
2. Multi-Layer Insulation (MLI) –Multi layer insulation are mainly used to reduce excessive heat loss from a component or also to isolate an excessively heat generating

system. The prime example is isolating a propulsion system from rest of the satellite to prevent back flow of heat into the satellite.

Figure 7-MLI with Aluminized Kapton coating [11].

3. Radiators- Radiators are used to dissipate excess heat. They are generally flat shiny surfaces with high values of emissivity and low values of absorptivity. Typical surface finishes include aluminized Teflon and white paints. Radiators can be used to dissipate excess heat from propulsion systems or to keep camera detectors cool.

2.3.2 Active control

Active Control - Active control systems use external power to produce the desired heating or cooling effect. These systems use solar energy to produce a heating or a cooling effect as they use batteries powered by solar energy to generate the desired effect. Active control systems are more complex and ideally thermal control of any space system should be achieved using only passive mechanisms.

1. Kapton Heaters-Kapton heaters are generally used for heating up sensitive components. They consist of a resistance element wrapped using Kapton films. The control mechanism involves using a temperature sensor and a controller to switch on or

off the heater. Kapton heaters have good space heritage and are also used aboard the International Space Station.

Figure 8-Kapton heaters. [12]

2. CryoCoolers- Cryocoolers are generally used for camera detectors to reduce the background noise generated at higher temperatures. Most detectors need an optimum temperature below the freezing point. Crycoolers are generally preferred when there is low structural vibrations present. There are various cryocoolers that work on the principle of Stirling Cycle or Reverse Brayton Cycle [13]. Thermoelectric coolers which work on the principle of the Peltier effect are also another type of cryocoolers currently in use for space applications.

3. Heat Pipes- Heat pipes transfer heat from electronics to the external surfaces or this heat can also be used to heat other components. Variable heat conductance heat pipes and loop heat pipes are amongst the commonly used heat pipes for larger spacecrafts.

Larger satellites travelling beyond Jupiter use Radioisotope Thermo electric generators to produce heat and to fulfill the power requirements of the space craft.

It is evident that traditional thermal control systems are not feasible solutions in a scenario with no solar energy and where low power electronics are used. A novel

mechanism that can produce heat without solar energy and without waste heat from the electronics is needed to sustain these low power electronics in extreme cold temperatures.

2.4 Thermochemical Energy Storage Systems (TCESS)

Thermochemical energy storage systems (TCESS) refers to chemical energy stored in the form of chemical bonds or micropores that can be released with chemical reactions or sorption processes. TCESS work on the principle of adsorption , absorption and hydration reactions . Adsorption reactions are surficial reactions that store energy in the micropores of the chemicals. Absorption reactions store the energy in the concentration difference of the diluted and concentrated salt solutions. Hydration reactions release heat when anhydrous hygroscopic salts form their corresponding hydrates. The commonly used terms in TCESS are listed in Table 1.

Sorbate	The liquid/ vapor phase chemical impinged on sorbent
Sorbent	The Solid/ liquid phase chemical used for energy release
Physisorption	Sorption without chemical bonding
Chemisorption	Sorption with chemical bonding

Table 1-Terminology for TCESS [14]

TCESS work on the principle of reversible reactions. Like a battery, they can be charged or discharged of thermal energy. The main processes taking place in a TCESS are explained below. [14,15]

Sorption (Discharging)- Adsorption or discharging refers to energy release when the adsorbate is in contact with the adsorbate top surface. In case of solid adsorption, energy is released due to energy released from Van Der Waal's forces which is also known as the binding energy. This is also known as dehydration and is an exothermic process.

Desorption (Charging)- Desorption involves heating the chemical using a heat source and get rid of the vapor stored in the chemical. For desorption to be done successfully, heating must be done at certain minimum temperatures depending on the working chemical and the ambient conditions like pressure, temperature. The minimum heating temperature is governed by the binding energy of the chemical at given ambient conditions.

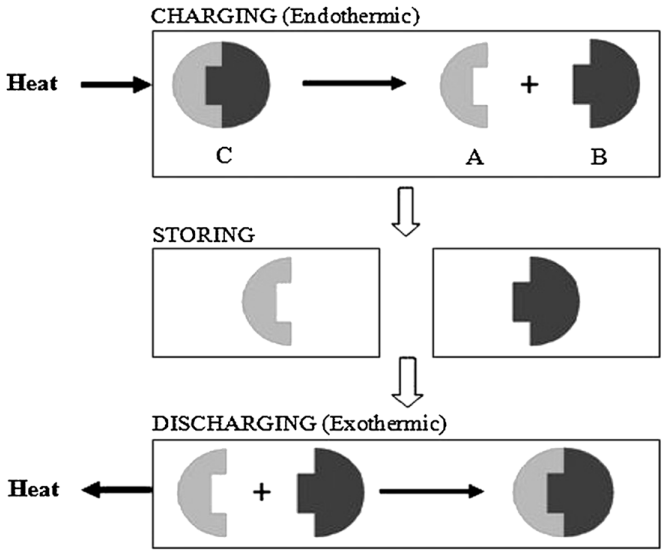

Figure 9- Principle of Thermochemical storage[15]

Furthermore, TCESS can be divided into two depending on the ambient pressures of operation.

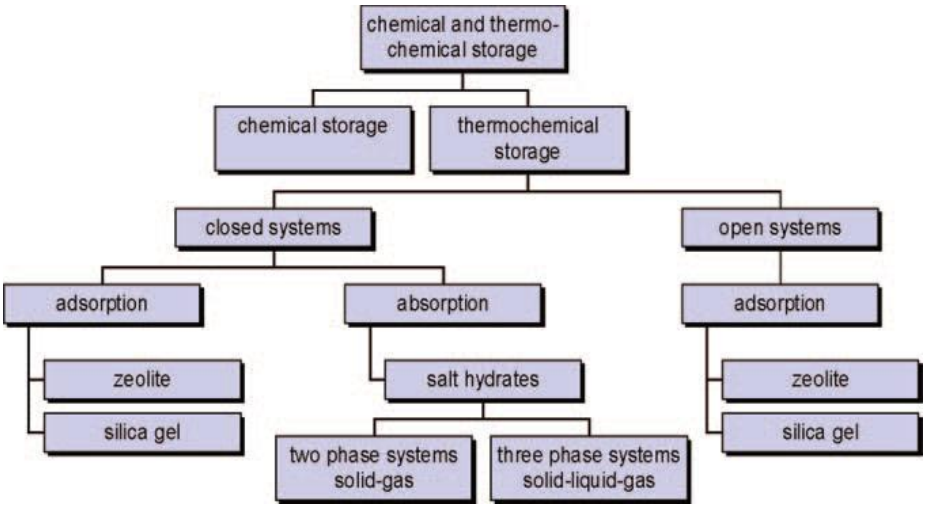

Figure 10-Types of Thermochemical Storage systems[16]

2.4.1 Closed Systems

In a closed system, the water released during desorption is used for adsorption purposes. External heat can be supplied to the sorbent using solar energy or in the form of steam heat. Closed systems are isolated from the atmosphere by having two chambers.

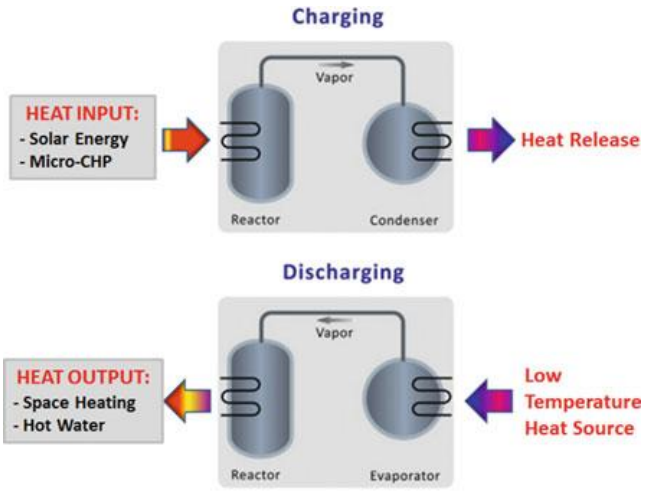

Figure 11- Working of a Closed System [14]

In one chamber, the chemically active sorbent is placed and a condenser/evaporator where the liquid/gas sorbate is placed. They are connected using pipes for transferring the liquid to the sorbent when required. During desorption, solar

energy incident on the sorbent releases the sorbent- sorbate attachments by overcoming the binding energy. This is then transferred to the condenser where the vapor is converted to liquid. The heat of condensation is transferred to a separate heating water loop. Closed systems are generally more complicated to build as they include evaporators and condensers used at different pressures. Typical applications include vapor adsorption coolers and heat pumps. [14]

In general, closed systems suffer from poor heat transfer characteristics due to addition of heat exchangers. These systems are more complex to design.

2.4.2 Open Systems

Open systems release the heat energy at atmospheric pressure. This is a simpler system design as it does not include heat exchangers and works at atmospheric pressure conditions [14].

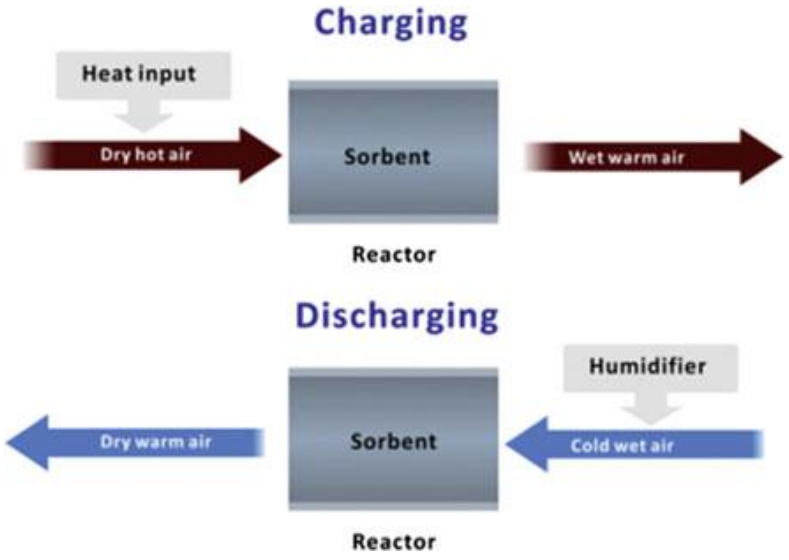

Figure 12- Working of an Open System[14]

Hygroscopic salts have limitations of operating in open systems. Lithium chloride for example has a critical humidity of 11 % at room temperature. This implies that Lithium Chloride requires only 11 % Relative Humidity (RH) at STP conditions to form an aqueous solution at room temperature. This makes the regeneration impossible at room temperature. To overcome this drawback, Composite materials have been studied. These materials have been manufactured for lab prototypes.

2.4.3 Selection Criteria

The selection of sorbents typically depends on number of factors. The crucial parameters are [17] :

1. High Water uptake
2. High Storage Density
3. Low charging temperature.
4. Fast reaction kinetics
5. Ease of availability
6. Ease of storage
7. Safety

TCESS have been used for long term solar energy storage. They have been widely used for heating of houses and buildings as well as for cooling of buildings. During the summer, the solar irradiance charges the thermos chemicals. The discharging reaction takes place in winter wherein the stored solar energy is used to heat water. Some of the widely used materials are Zeolite 13X and lithium chloride. The charging temperature is

the most influential characteristic as it determines the power and quality of the energy source [17].

Figure 13-Zeolite 13X beads.

Zeolites are naturally occurring or synthetically manufactured alumino-silicates. Zeolite 13x has a one of the highest energy densities and heat of adsorption for open systems [18]. A 7000 kg Zeolite 13X system was installed in Munich to provide heating in a school. This open adsorption system provides 135 kWh/m^3 of energy storage density[19]. Zeolites are preferred for open systems as they are not hygroscopic due to their electrostatically charged framework. They are hydrophilic in nature. As a result though they have relatively high storage densities, they also need much higher regeneration temperatures. The hydrophilicity can be varied by changing the Silicon to Aluminium Ratio [20]. Some of the projects reviewed in this survey are listed below.

Chemical Pair	Type	System	Charg. Temp.	Storage Density(Kwh/m^3)	Storage Density(Kwh/kg)
$LiCl/H_20$[39]	Liquid Absorption	Close	65.6	400	1219
$LiBr/H_20$[39]	Liquid Absorption	Close	72	313	561
Na_2S/H_20[40]	Chemical Reaction	Close	72-83	780	1070
$MgSO_4/H_20$	Chemical	Open	150	924	694

	Reaction				
$MgCl_2/H_20$	Chemical Reaction	Open	130	556	477
$SrBr_2/H_20$	Chemical Reaction	Close	80	175	250
Zeolite 4A	Solid Adsorption	Open	180	98-173	140-223
Zeolite 13X	Solid Adsorption	Close	180	110	149

Table 2-Data of selected thermochemical projects[17]

This technology has attracted interest from the space community for cooling purposes. A High-Capacity Spacesuit Evaporator Absorber Radiator (SEAR) for manned space exploration space crafts has been proposed. The system was designed to provide a cooling effect of 293K by rejecting heat with only radiation at 323K. [21]

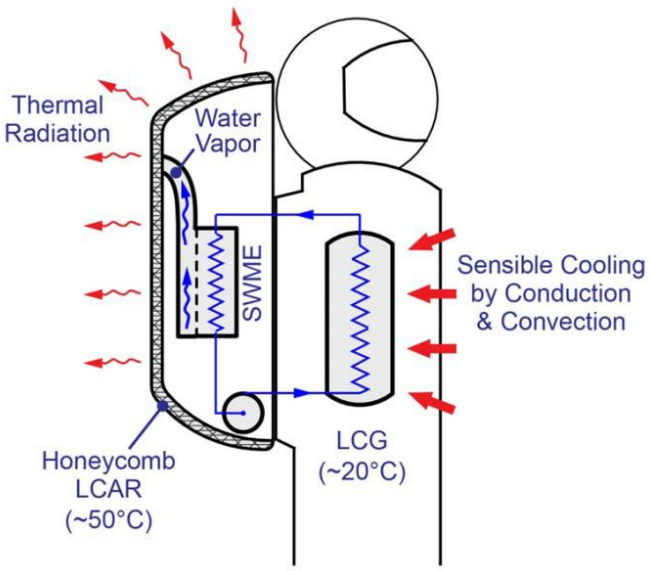

Figure 14- SEAR design[21]

The system consists of a lithium chloride based heat rejection system coupled with a water membrane evaporator for heat gain. The aim of this technology is to help humans in extreme conditions. The main issue with pure chemicals as a material is the influence of Deliquescence Relative Humidity (DRH). If DRH increases beyond Relative Humidity

of the system, a salt solution will be formed. In this case regeneration of the salt becomes a huge issue. This is a problem especially for open systems[17]. In closed systems it is possible to maintain the relative humidity of the system within desired limits by using a coolant.

2.5 Composite Materials

Most pure chemicals have poor mass transfer characteristics and are poor conductors of heat[14]. Pure chemicals can be prepared with composite materials to increase effective thermal conductivity of the material and improve chemical reaction kinetics. They can overcome pressure drop across the salt bed and hence reduce energy required for regeneration purposes. They also assist in overcoming the DRH problem. Some materials increase hydrophilicity of the salts and thus increase water uptake. Nonnen et al prepared 100 L of Zeolite X and 15% by wt. Calcium chloride composite and proved a 68 % increase in storage density compared to traditional Zeolite X [22]. A composite mesoporous honeycomb element based on Wakkanai siliceous shale (WSS) and lithium chloride (LiCl) was developed and used as an open absorption system and reported a storage energy density of 50 Kwh/m3. WSS is mixture made primarily of Silicon Oxide. This material improved the hydrophilic nature of the thermochemical composite. Silicon however has low thermal conductivity. The heat transfer characteristics is reduced as a result. This research though proved that the mass flow rate of the air also changes storage density. The calculated storage density increased from 35 kwh/m^3 to 50 kwh/m^3 as the air flow increased from 1m^3/hr to 3m^3/hr . [23] To improve the performance, further, a composite of LiCl and activated carbon was fabricated.

Carbon at the micro and nanoscale exhibits a very high thermal conductivity. Using this material, a storage density of 1250 Wh/kg was achieved. [24]

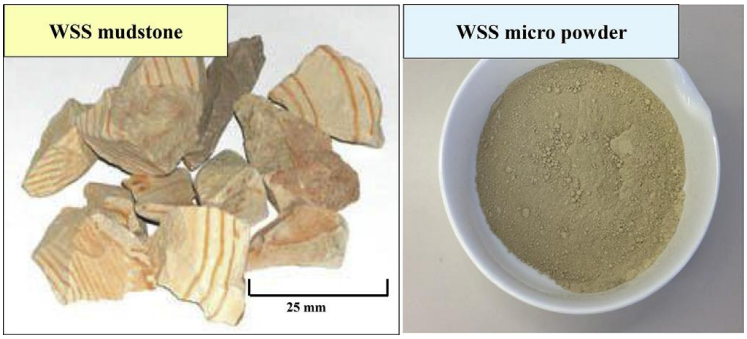

Figure 15-WSS powder [23]

All these systems have been developed for large scale applications. In summary it is important to note that the energy density storage is a system property and not a material property [25].Each storage material will thus have a different performance at different ambient conditions.

The ambient conditions and the properties of the sorbate will affect the energy released. The vapor/liquid transport phenomena will be governed by the ambient pressure. At lower pressures, the transport of the sorbate through the sorbent bed will be better and more efficient for closed systems. It implies that every chemical will have a different storage density at different operating conditions. Thermochemical storage provides an almost *loss free storage system* as energy is not stored in the form of sensible energy. This makes it a great candidate for long term thermal storage solutions.

CHAPTER 3

METHODOLOGY

3.1 System Overview

The sensor module will consist of science and communication electronics along with the PEM fuel cell and the TCESS.

The water required for the hydration reaction will be supplied by the PEM fuel cell. In vacuum the output from the fuel cell will be vapor and not liquid water. It is essential to control this flow rate to get the optimum performance from the TCESS. If the sensor module is vacuumed, a pressure difference will be necessary to facilitate the flow of vapor. A temperature sensor will govern this system and the flow control valve will open at only the set temperature. The DC-DC converter will be necessary to supply a constant current at a specified voltage from the fuel cell.

3.2 System Design

The system design consisted of two concentric spheres with the inner sphere housing the electronics and power supply. This kind of design was chosen as it minimizes heat loss. The inner sphere is divided into three parts. The top part contains all the electronics and the middle part contains the power source. The lower part is empty and is designed keeping in mind potential storage of Lithium Hydride.

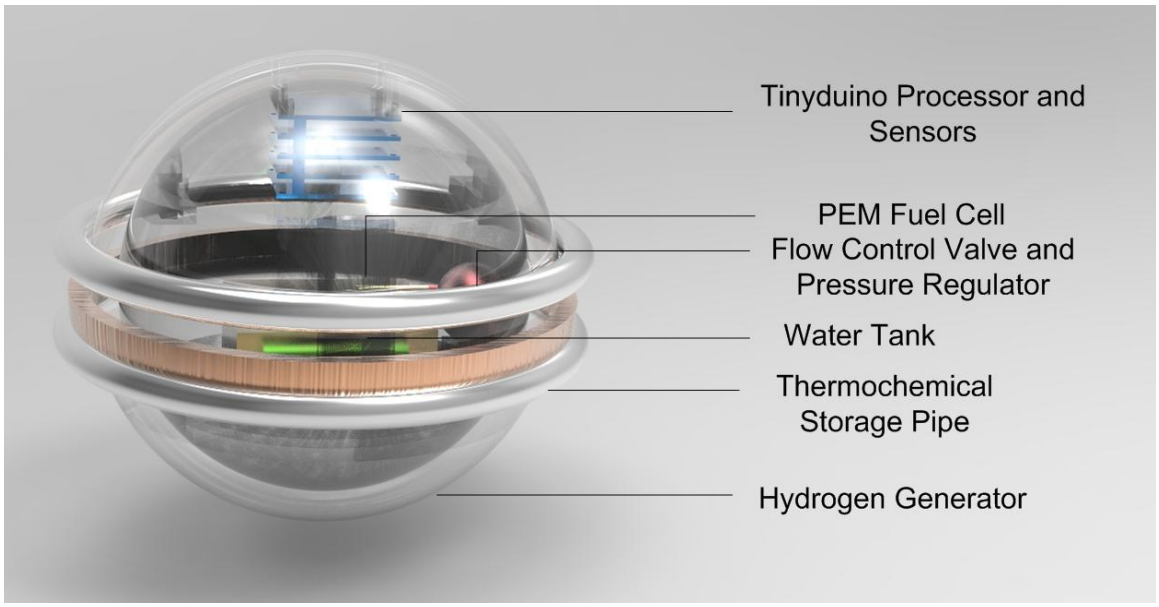

Figure 16-Proposed Design of inner sphere

The thickness of the inner sphere was kept 5mm. The higher thickness also increases conduction resistance thereby reducing rate of heat loss. The design consisted of using slots to connect the three parts of the inner sphere. This is a simple technique. In case the gap between the two spheres is to be vacuumed, silicone gaskets and high accuracy press fit slots will be needed to ensure the vacuum does not fail. The spheres are connected using a circular connector ring.

Figure 17- Connector Ring

The inner sphere is press fitted into the ring and then the ring is attached to the outer spheres using simple slots. This technique does not require welding or additional mechanical parts. The outer sphere was divided into two parts and screws were used to join the parts. This forms the basis of experiment without using thermochemical storage materials.

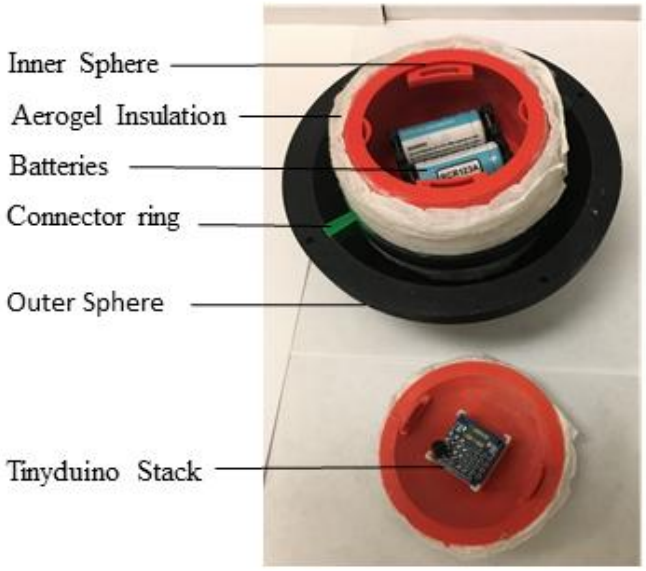

Figure 18-System Layout

When thermochemical storage material is used, it is placed in a hemispherical container surrounding the inner sphere. Water is discharged using a syringe and tube system. The mass flow rate is not calculated.

The mass budget of the system is presented in the table below.

Subsystem	Component	Mass(g)	Max. Deviation	Max.Mass(g)
Structure	Outer sphere	178	1.2	213
	Inner Sphere	102	1.2	122
	Connector ring	5	1.1	5.5

	Battery Holders	19	1.1	201
	TCM container	21	1.1	23.1
Command & data Handling	Tiny duinoProcessor	4	1.1	4.4
	SD card module	4	1.1	4.4
Communication	Tinyduino comms. board	7	1.1	7.7
Sensors	BMA 250	4	1.1	4.4
	TMP 36	2	1.1	2.2
Power	Battery	25	1.3	32.5
Thermal	Insulation	3	1.1	3.3
	TCM salt	25	1.2	30
Miscellaneous	Nuts	3	1.2	3.6
	bolts	2	1.2	2.4
Total				480

Table 3-Mass Budget

3.2.1 Electronics

Electronics used inside were Tinyduino circuits. Tinyduinos' are smaller versions of Arduino microcontroller's with the same processing power at lower clock frequency. Arduinos' are space qualified having been used aboard the ArduSat. For a PEM fuel cell a DC-DC converter will be necessary. The electronics used inside are listed below.

Electronic Component	Function
Tinyduino Processor	Command handling board
Tinyduino Sensor module	Collect temperature, accelorometer data
Tinyduino SD card module	Data storage
Tinyduino break out board	Required for TMP 36 sensor
Tinyduino motor drive	Required for Kapton heater
TMP 36 Temperature Sensor	Collect Temperature data.
Kapton heater	To compare performances of heater and thermo chemical

Table 4- List of Electronics[26]

In the module a 3.7 V lithium ion battery was used to supply the power and replicate the effect of a fuel cell. The Kapton heater and the tinyduino motor drive are not

part of the proposed design. The Kapton heater is used to see difference in the performance compared to the chemicals. Kapton heaters are generally used in space systems for component heating. 12V is the most common voltage bus used for satellites and hence that heater was used. A kapton heater was setup using a non-rechargeable secondary battery of 9V to compare the performance with TCESS. The motor drive powered by the tinyduino is used to run the heater. A 9V battery had to be used because of the space constraints in the module. The heater does not run at full power but sufficiently high to get the desired heating effect. The heater also cannot be used above 11V as that is the limitation factor imposed by the motor drive [27] . The TMP 36 sensor and the tinyduino sensor module are used to record temperatures. The tinyduino temperature sensor BMA 250, has a sensitivity of 0.5^0C and the TMP 36 sensor has a sensitivity of 0.1^0C [26,28]. The TMP 36 sensor is placed near the centre of the inner sphere. The BMA 250 is placed at the periphery.

The heater is controlled using a PID controller . The values for the proportional gain, integral gain and differential gain were found by auto-tuning the heater. The auto-tuning of the heater is done by placing the module in the necessary freezing conditions and the code generates the optimum gain parameters. The TMP 36 sensor as well as the tinyduino temperature sensor data are used to store the temperature data.

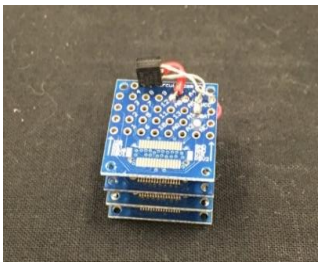

Figure 19-Tinyduino Stack

3.2.2 Power Budget

The power budget of the system lists the power generated by each component within the system. It also informs the maximum power generation capacity of the system. All components reject heat to the environment due to operational inefficiencies. Every component has its individual losses depending on function. In the sensor module, all electronics are low power devices. The SD card requires the maximum current of 100 mA [26]. The cylinder type lithium ion battery has a discharge efficiency of 85 % at room temperature.

Component	Current(mA)	Voltage(V)	Power generated(mW)	Heat lost(mW)
Processor	1.2	3.5	4.2	0.42
SD Card	100	3.5	350	35
Sensor board	0.14	3.5	0.49	0.049
TMP 36	0.05	3.5	0.175	0.0175
Total			355	35
Battery			355	53
Total Power Lost				88

Table 5-System Power Budget

The low power electronics also have inefficiencies associated with them. A 10 % heat loss is assumed for all electronics. The SD card module consumes 0.35 W only when it records the data. Since data is being recorded at every 10 seconds, this value is assumed to be constant over the entire time the experiment is run.

3.3 Experimental Procedure

The tests are conducted at 32 ± 1 ^{o}C in a freezer . This temperature is chosen keeping in mind the electronics have an operational temperature range up to -35 ^{o}C. Based on the performance , experiments were extended to -40 ^{o}C. The procedure is as follows :

1. The Aerogel blanket is attached to the external surface of the internal sphere. The blanket is attached using adhesive. The sphere is wrapped in single layer of aluminum foil.
2. The electronics are mounted in the top sphere and the battery is fixed in the middle sphere. The electronics and data logger is turned on.
3. The three parts of the sphere are fixed together.
4. The connector ring is press fitted onto the aerogel covered inner sphere. The connector ring is fitted into the slots on the periphery of the external sphere. This connects the inner sphere and lower outer hemisphere.
5. The outer hemispheres are covered in Aluminum foil.
6. The TCM container is then placed on the inner sphere. The TCM container has notches to ensure the thermochemical bed is non- uniform. This will help to increase the water diffusion through the bed.

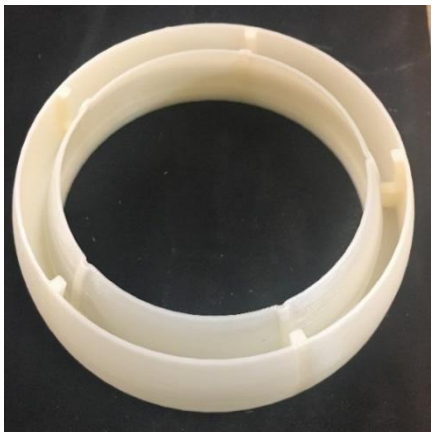

Figure 20-TCM container

7. Cold water is then sprayed on the TCM. The container is closed using a lid.
8. The upper outer hemisphere is connected to the lower outer hemisphere using M3 nuts and bolts
9. The module is placed in the freezer for 8 hours.
10. After 8 hours the system is removed from the freezer and the data from the SD card is retrieved on the computer.

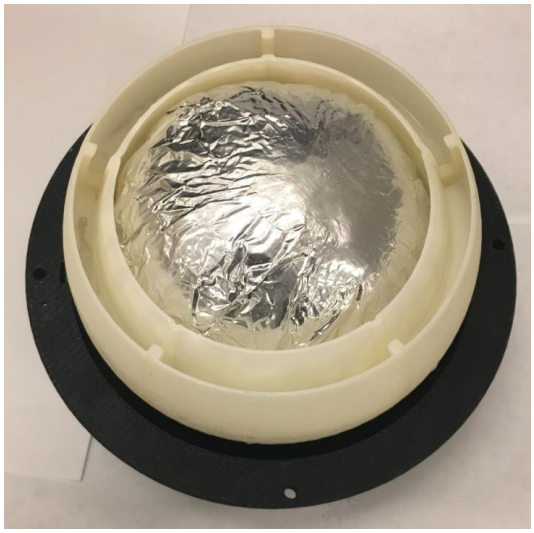

Figure 21-Experimental Setup for sensor module

Steps six and seven are done only when the performance of the thermochemical storage system is to be verified. In case of the heater and TCM comparison experiment, the heater and its battery are mounted in the middle sphere along with the rechargeable battery used to power the Tinyduino processor.

3.3.1 Thermochemical storage material experiments

Thermochemical experiments were performed to primarily understand behavior of the chemicals at low mass, low water temperatures and at low ambient temperatures. The table top experiments were separately performed using a fluke temperature sensor, a mass scale and simple beakers. The experiments were performed for 15 minutes. These experiments should ideally be performed at various pressure as water uptake and latent heat of vaporization is different at every pressure. This was not done in this work. Chemicals are chosen based on their theoretical energy storage density at STP conditions. Experiments were performed for 15 minutes as this is enough time to gauge the performance in terms of maximum temperature reached and subsequent fall in temperature. The energy released depends on the adsorption energy and the energy required to retake the performance depends on the desorption energy. The performance of a thermochemical depends on the ambient conditions, initial conditions as well as sorbate temperature. Water is used as the sorbate. The quantity of water is 25 ml. The rate of water production is given by, [29]

$$Q_w = 9.34 \times 10^{-8} \times \frac{P_e}{V} (\text{kg/sec}) \quad (1)$$

Where,

P_e = Power capacity of fuel cell (W)

V= Max. Voltage provided by fuel cell (Volt)

3.3.2 Experimental Procedure for Thermochemical storage material

1. Measure the required quantity of water in a beaker. Ensure temperature is 0 ^{o}C
2. Measure the required quantity of sorbent in beaker. Ensure steady state temperature of -20 ^{o}C is attained.
3. Immerse sensor in the sorbent.
4. Pour water and keep setup in -20 ^{o}C.
5. Record temperature data using the fluke multimeter.

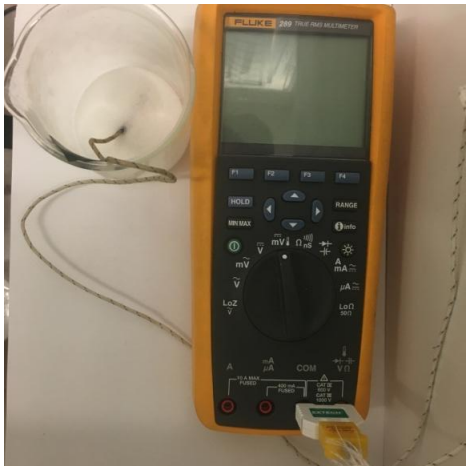

Figure 22- Experimental Setup for TCESS testing

The table top experiments are a simple way of determining the optimum water requirement. The heating effect produced depends on the water quantity. The heating effect provided will depend on the geometry of the TCM container. It

will be independent of the sensor module geometry. The thermal model hence does not include the effect of the TCESS .

CHAPTER 4

THERMAL SYSTEM DESIGN

4.1 Thermal System Materials

4.1.1 Insulation Material

To achieve the thermal control objectives, thermal materials were chosen based on space heritage. Aerogel blanket was chosen as the insulation material supplied by Cabot Aerogel. It has a thermal conductivity of less than < 0.1 W/mK and is lighter than air[30]. Aerogel insulation was applied only on the inner sphere as theoretical modeling showed negligible effect of applying insulation on the outer sphere as well.

Figure 23-Aerogel Thermal Blanket

4.1.1 Surface Coating

Surface coatings are used to vary optical properties such as emissivity and absorptivity. It is essential to low emissivity surface coatings on exterior sides of both spheres. In space systems, Aluminized Kapton and Goldized Kapton are the preferred materials to reduce emissivity [10]. Aluminum foil was also used to reduce the emissivity

values of the surface. Although the preferred material is Kapton, aluminum foil is cheaper option and more easily available. Aluminum foil was used on exterior surfaces of both spheres to reduce emissivity. The inner surface of the outer sphere was left unchanged as black provides the highest emissivity. This ensures the inner surface radiates maximum heat to the inner sphere.

4.2 Steady State Thermal Model

In the steady state thermal model, all three forms of heat transfer namely conduction, convection and radiation exist. The advantage of the steady state model is that it is independent of mass and specific heat which if assumed wrong will lead to inaccuracies in the final result. The thermal design of the system without thermochemical storage system was done. For a spherical geometry, a 1D lumped capacitance model was created. The model is done assuming terrestrial conditions and hence convection heat transfer also exists.

The steady state model is based on law of conservation of energy. At each node this law is applied and can be expressed as,

$$Q_{gen_i} + Q_{in_i} = Q_{out_i} \quad (2)$$

Where,

Q_{geni} – Internal heat generation at node *i* (W)

Q_{in_i} - The heat input at node *i* (W)

Q_{out_i} -The heat leaving node *i* (W)

The power input at each node can be found using thermal resistances. The expression is given as,

$$Q = \frac{\Delta T_{ij}}{R_{ij}} \qquad (3)$$

The model has total seven nodes with the seventh node being the boundary node with a constant temperature constraint. This represents the ambient temperature. Figure 25, 26 and Table 5 explain the position of each node. The following important assumptions were made in the model:

1. The thermal conductivity is assumed constant and isotropic.

2.Surface emissivity is assumed constant and effect of surface roughness is not taken into account.

3. The conduction loss between module and the refrigerator cabin is neglected.

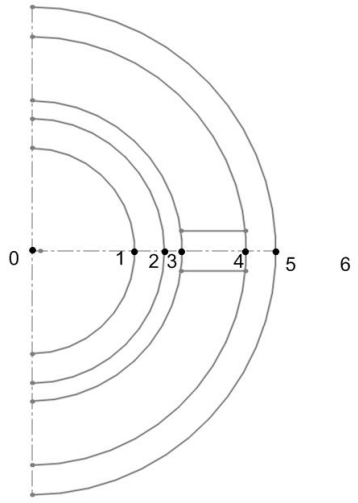

Figure 24-Position of Nodes

Node	Location
0	Inside inner sphere
1	Inner side of inner sphere
2	Outer side of inner sphere
3	Inner insulation
4	Inner side of outer sphere
5	Outer side of outer sphere
6	Ambient temperature

Table 6-Position of Nodes

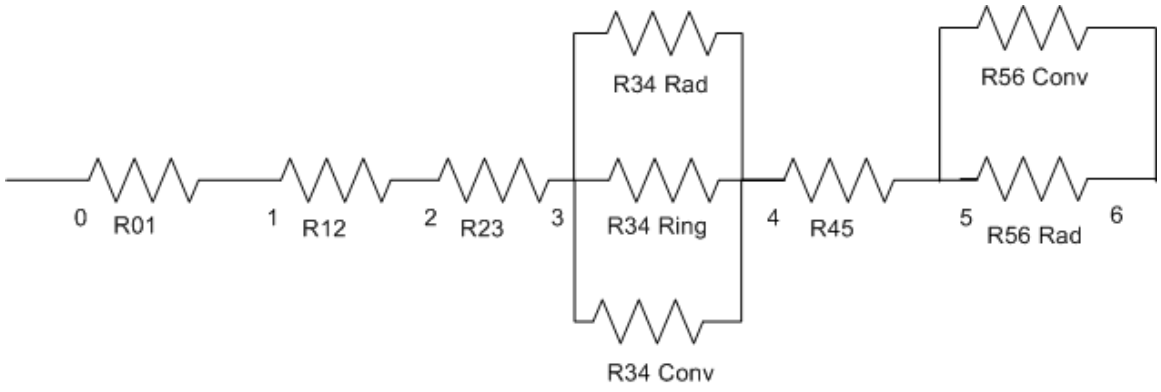

Figure 25-Equivalent Resistance Network

For calculation, radiation between node zero and node one was neglected to reduce computation time. This does not affect the theoretical model much as at any given point in time, the temperature difference between these two nodes is very less. Node zero represents the internal component temperature of the sensor module. A single node is a sufficient approximation on account of low internal power generation and small gap between the SD card module and battery, which are the prime heat producers. Surface to surface radiation was assumed between node three and node four to increase accuracy of the model. There is also conduction between node three and four due to presence of connecting rings. As all three modes of heat transfer occur simultaneously between the same two nodes, these resistances are in parallel. Parallel resistances decrease the overall resistance thus increasing heat loss. It is very difficult to further reduce the conduction and convection losses between these two nodes. Aluminum foil and black paint is used to reduce the radiation losses. The overall gain though should be minimal as conduction and convection losses are much larger compared to radiation losses. In the model outer insulation was not used as the temperature profile did not greatly differ with or without insulation. By assuming a node at every interface, it is possible to get the most accurate thermal model.

The steady state thermal model is a non-linear system of simultaneous equations. The solution will return temperatures at every node and the temperature should decrease as interior nodes move towards the ambient temperature node. The values used for the analysis are listed below.

The system was solved using the modified Newton-Raphson method at nodes where radiation is involved and standard linear equations at nodes where radiation is not involved. The thermal resistances are given as,

$$R_{01} = \frac{1}{h_1 A_1} \tag{4}$$

$$R_{12} = \frac{\ln (r_1 / r_2)}{4\pi r_1 r_2 k_{abs}} \tag{5}$$

$$R_{23} = \frac{\ln (r_2 / r_3)}{4\pi r_3 r_2 k_{ins}} \tag{6}$$

$$R_{34ring} = \frac{L}{2k_{abs}\, A_{ring}} \tag{7}$$

$$R_{34Rad} = \frac{1}{\varepsilon_3} + \frac{1-\varepsilon_4}{\varepsilon_4}\left(\frac{r_3^2}{r_4^2}\right) / \left(\sigma A_3 (T_3 + T_4)(T_3^2 + T_4^2)\right) \tag{8}$$

$$R_{34conv} = \frac{1}{h_1 A_3} \tag{9}$$

$$R_{34total} = \frac{R_{34conv} R_{34Rad}\, R_{34ring}}{R_{34Rad}\, R_{34ring} + R_{34Rad}\, R_{34conv} + R_{34conv} R_{34ring}} \tag{10}$$

$$R_{45} = \frac{\ln (r_4 / r_5)}{4\pi r_4 r_5 k_{abs}} \tag{11}$$

$$R_{56rad} = \frac{1}{(\sigma \varepsilon A_5 (T_5 + T_6)(T_6^2 + T_5^2)} \tag{12}$$

$$R_{56conv} = \frac{1}{h_2 A_5} \quad (13)$$

$$R_{56total} = \frac{R_{56conv} R_{56rad}}{R_{56conv} + R_{56rad}} \quad (14)$$

Variable	Value	Units
r_1	0.035	m
r_2	0.040	m
r_3	0.043	m
r_4	0.055	m
r_5	0.060	m
A_1	0.015	m^2
A_2	0.020	m^2
A_3	0.023	m^2
A_6	0.045	m^2
L	0.010	m
ε_1	0.1	-
ε_2	0.7	-
ε_3	0.1	-
h_1	1	W/m^2K
h_2	2.65	W/m^2K
K_{mat} [33]	0.50	W/mK
K_{ins}[30]	0.02	W/mK

Table 7-List of variables

The natural convection heat transfer co-efficient (h) ranges from 1-10 W/m^2K [10]. For a domestic refrigerator, this value was reported to be $3W/m^2K$[30]. The natural convection heat transfer co-efficient can be used using the following Nusselt number relation.This methodology gives value of 2.94 W/m^2K

$$Nu = 2 + \frac{0.589Ra^{0.25}}{[1+(0.469/Pr)^{9/16}]^{4/9}} \quad (15)$$

The Rayleigh number Ra, is given by,

$$Ra = \frac{g\beta(T_s - T_{amb}){L_c}^3}{v^2} Pr \quad (16)$$

$$\beta = \frac{2}{(T_s + T_{amb})} \quad (17)$$

$$h = \frac{Nu \times k}{L_c} \quad (18)$$

L_c is the characteristic length and it is the diameter for a sphere. The Prandtl number Pr, and kinematic viscosity υ can be found from literature data and is 0.7335 and 1.426*10e-5 m^2/s respectively. The thermal conductivity k is 0.024W/mK. This methodology of finding the natural heat transfer co-efficient is valid only for $Ra \leq 10^{11}$ [32].The natural heat transfer-co-efficient at the external surface of the external sphere can be found using this method. The heat transfer between concentric spheres is assumed a minimum value of 1 W/m^2K as the standard empirical relation available from literature does not apply to the model presented here.[32]

4.3.1 Comparison of Sphere and a Cube

Along with a sphere in a sphere, a cube in a cube configuration was also considered. A cube has a larger surface area to volume ratio than sphere, making it necessary to generate more heat for a cube than a sphere to maintain the same steady state temperature. It is easier to mount the components in a cube because of flat surfaces. It is easier to efficiently utilize the volume in the cube. The thermal model remains similar as a cube is also symmetric along all axes. The conduction formula will change and the formula for heat conduction through a wall is used. The graph and table below indicate the variation in steady state temperatures with change in ambient temperatures, heat

generated for both cube and a sphere. For a sphere of 35 mm , the equivalent cube side is 56.4mm.

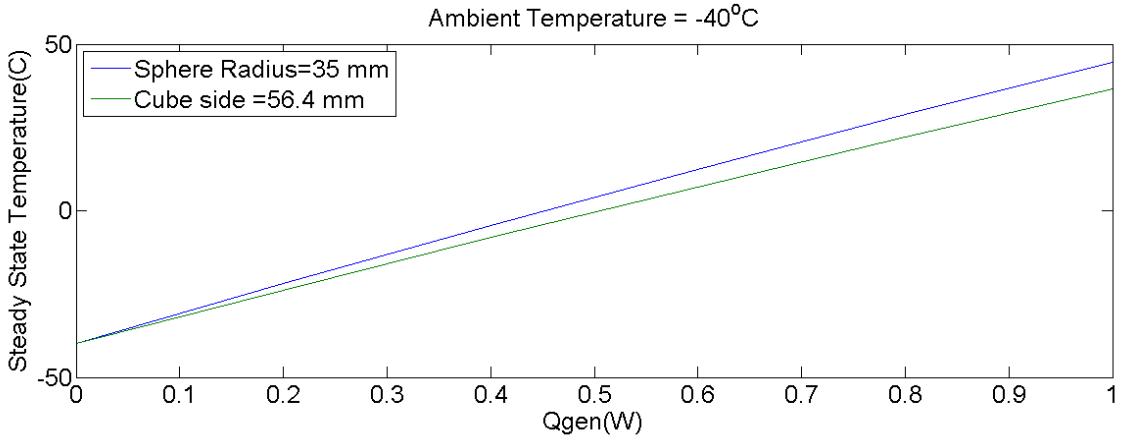

Figure 26- Comparison of Sphere and Cube

The graph shows the comparison of the power generation requirement for a sphere and a cube for space environment. A cube requires more heat due to its larger surface area. The difference in power requirement increases with increase in size of the module for any ambient temperature. From the data , it is clear that a sphere has better heat retention capacity than a cube. Hence a sphere in a sphere configuration was chosen for the module.

Ambient Temp(C)	-120°C		-80 °C		-40 °C	
	Steady State Temperature(C)					
Heat Generated(W)	Sphere	Cube	Sphere	Cube	Sphere	Cube
0.2	-87	-91	-57	-59	-22	-24
0.4	-60	-66	-35	-40	-4	-8
0.6	-36	-44	-15	-22	13	7
0.8	-15	-25	4	-5	29	22
1	5	-6	21	12	45	37

Table 8- Comparison of spherical and cubical sensor module

The trends inferred from the table are

- The difference in steady state temperature for a sphere and a cube decreases with increase in ambient temperature.
- The difference in steady state temperature increases with increase in generated power.
- The above trends exist as at lower ambient temperatures; the radiation losses are more significant as the temperature gradient is larger. As a result a small change in area has a greater influence on the steady state. As the power increases, the losses will increase and impact of a larger area will be more significant.

4.3.2 Variation of temperature with Sphere Radius

Having determined the benefits of a sphere in a sphere configuration over a cube in cube configuration, the optimum size of the sphere is found using the same thermal model. The sphere size is crucial from a thermal design perspective. Initially, a sphere of inner radius 25mm was chosen. It proved difficult to fit all the components in that form factor. The sphere of radius of 35 mm was chosen as it allowed us to fit the battery in the middle section of the inner sphere. The outer radius of the sphere is kept 20mm greater than the inner sphere in all cases. The surface plot shows the variation of steady state temperature with power generated and with inner sphere radius for ambient temperature of -40^0C.

Sphere Radius / Heat Generated(W)	0.030m	0.035m	0.040m	0.045m
	Steady State Temperature(C)			
0.2	-17	-22	-25	-28
0.4	5	-4	-11	-16

0.6	26	13	3	-4
0.8	47	29	16	7
1	66	45	29	18

Table 9- Performance of module with different radii's.

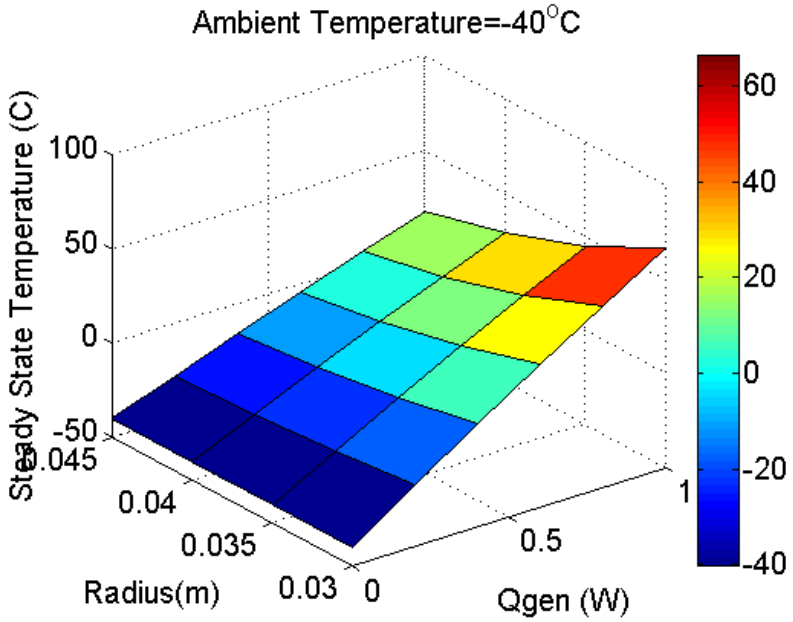

Figure 27- Surface plot comparing steady state temperatures of sphere at various amb. Temperatures

4.3.3 Comparison of predicted performance on Earth and in Space.

The experiments of the sensor module performance were done on earth. The difference in the predicted performance in space and on earth is shown in the graph and table below.

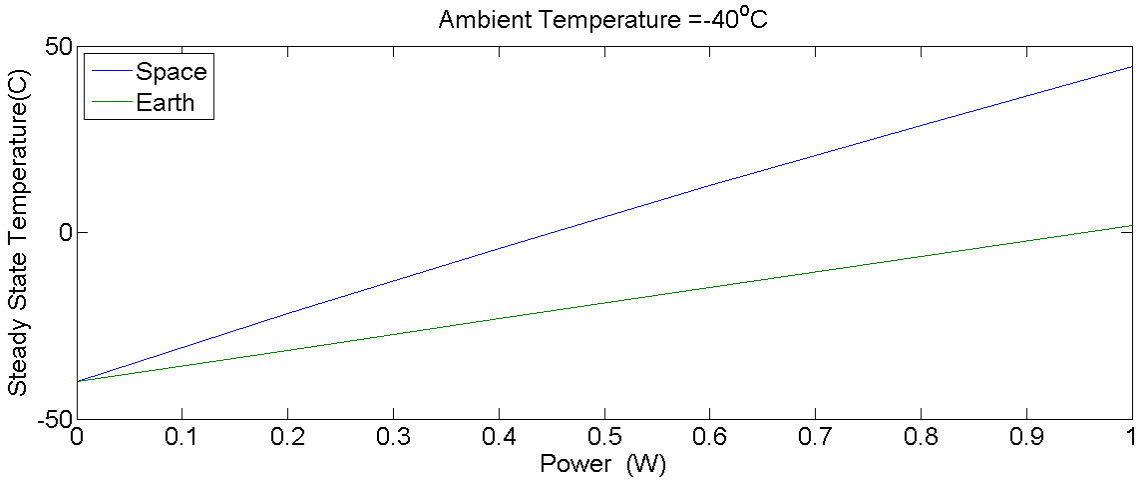

Figure 28- Performance in Space and on Earth

The table shows variation in steady state temperatures on earth and in space with change in ambient temperature and the power generated for sphere of inner radius of 35mm.

Qgen Amb.T(C)	0.2 W		0.4 W		0.6W		0.8W		1 W	
	Earth	Space	Earth	Space	Earth	Space	Earth	Space	Earth	Space
-120	-107	-87	-94	-60	-82	-36	-69	-15	-56	5
-80	-67	-56	-55	-35	-43	-15	-30	4	-18	21
-40	-28	-22	-16	-4	-4	13	8	29	20	45

Table 10-Comparison of performance on Earth and in Space

The following trends are observed from the table:

1. For any ambient temperature, when the same power is generated, the steady state temperature in space is always higher. This is due to lack of convection losses in space.

2. The difference in steady state temperatures for earth and space increases with increase in power generation for constant ambient temperature.

3. The difference in temperatures decreases with increase in ambient temperature for given power generation.

4. To achieve the same steady state temperatures at a given ambient temperature, the power generation factor needs to be increased by factor of greater than two for earth condition. This factor reduces to less than 1.5 with increase in ambient temperature.

4.3 Transient Thermal Model

The transient temperatures can be found out using the following system of ordinary differential equations. This system can be solved using Matlab's ODE45 function. It is essential to have a separate system for steady state conditions because computing using ODE 45 is time consuming particularly given the inherent nonlinear dynamics associated with radiation heat transfer. The system of ordinary differential equations is given by

$$mc_p \frac{dT}{dt} = Q_{gen_i} + Q_{in_i} - Q_{out_i} \quad (18)$$

According to the model every node is only connected to the node preceding it and to the node after it. The heat generation term will exist only for the first node and it is the total heat lost value from the power budget. The heat input of any node *i* is given by the conduction, convection and radiation losses of the preceding node or the $(i-1)^{th}$ node... Specific heat is a material property and is found from the relevant data sheets. The mass budget gives the mass at each node. As the nodes are placed at the boundaries , there are two nodes each associated with the spheres. The mass is distributed evenly at each node. The rate of temperature drop of the system depends on the thermal time constant of the

system. The thermal time constant is a function of the internal heat generation, thermal inertia and thermal resistance of the system.

4.4 Energy Storage Principle

For a sorbate-sorbent system, during desorption, the binding energy and heat of evaporation along with the sensible heat to heat up to boiling point must be supplied [34]

$$Q_{char} = Q_{sens} + Q_{evap} + Q_{bind} \quad (19)$$

Where,

Q_{char}- Charging Energy

Q_{sens}- Sensible Energy

Q_{bind}- Binding Energy

Q_{evap}- Energy of Vaporization

In case of sorption process, this energy is only the sum of the heat of evaporation and binding energy. For short term storage, as sensible heat losses will be less the sensible heat to be supplied during desorption will reduce. For long term storage, owing to larger sensible heat losses the energy to be supplied will be larger.

In case of hydration reactions, the heat of formation can be used to estimate the energy storage density [35]. The heat of reaction for any reaction is given by:

$$\Delta H_R = \sum H_{f_{products}} - \sum H_{f_{reactants}} \quad (20)$$

The heat of formation is calculated at STP conditions. As enthalpy is a function of both temperature and pressure, the heat of reaction changes accordingly. For multiple step reactions the heat of reactions of every step are summed to get the total heat of reaction

[35]. Although the approach is straight forward, at different ambient conditions, the steps associated with each reaction is different and it is difficult to tabulate these steps at different conditions. The heat of reaction is a theoretical value which can be attained only in an ideal process. Practically, the heat of reaction also depends on surface properties of the salt as they depend on mass transfer of the vapor to generate heat which is not taken into account in the above formula.

CHAPTER 5

RESULTS AND DISCUSSION

5.1 Thermochemical Selection

Based on the literature review, lithium chloride was chosen as the chemical for storage and release of heat for the experiments. Lithium chloride hasn't been used in open systems so far as it has low critical relative humidity. It is used in closed systems as an aqueous solution . The table gives a glimpse of heats of reactions at STP conditions of some chemicals for hydration reactions. Negative energy indicates an exothermic reaction. The Nomenclature is as follows

$\Delta H_r = \text{Heat of reaction (kJ/mol)}$

$\Delta H_{fd} = \text{Heat of formation of dehydrated salt (kJ/mol)}$

$\Delta H_{fh} = \text{Heat of formation of hydrated salt (kJ/mol)}$

$\Delta H_{fh} = \text{Heat of Formation of water vapor} = -241.8\ \text{kJ/mol}$

x- Number of moles of water.

The heat of reaction is calculated using the following formula:

$$\Delta H_r = \Delta H_{fh} - (x\Delta H_W + \Delta H_{fd}) \quad (21)$$

This formula assumes all reactions are single step reactions.

Dehydrated Salt	ΔH_{fd}	Molar mass(g/mol)	Hydrated Salt	ΔH_{fh}	ΔH_r	Energy Storage (wh/kg)
LiCl	-408	42.4	$LiCl.H_20$	-712	-56	369.8
LiCl	-408	42.4	$LiCl.2H_20$	-1013.7	-109.7	724.4
LiCl	-408	42.4	$LiCl.3H_20$	-1311	-159	1050
LiCl	-408	42.4	$LiCl.5H_20$	-1889.11	-241.11	1592.24
$MgSO_4$	-1278	120.36	$MgS0_4.7H_20$	-3388	-374	870.0
$MgCl_2$	-641	95.21	$MgCl_2.6H_20$	-2499	-370	1088.10
$SrBr_2$	-717	247.4	$SrBr_2.6H_20$	-2531	-326	368.91
$CaCl_2$	-795	110.98	$CaCl_2.6H_20$	-2607	-363.2	911

Table 11-Trade Study of Thermochemicals

Lithium chloride forms stable dihydrate and trihydrate crystals in the temperature range of 233K-293K. Table 10 indicates that Lithium chloride has higher water intake at these temperatures and hence higher heats of formations [36].

Figure 29-Lithium Chloride

It is essential to carry out experiments to understand the behavior of lithium chloride and water interaction under different conditions. As discussed earlier, the behavior of each chemical is different in different operating conditions. As a result, the heating produced by lithium chloride will be different in vacuum conditions.

5.2 Variation of thermal performance with Ambient Temperature and Water Temperature.

Experiments were performed to check the performance of 25 gm of lithium chloride in ambient temperature of -20^{o}C and with water temperature of 0^{o}C. The water quantities chosen were 15ml and 25 ml. The graph is plotted below.

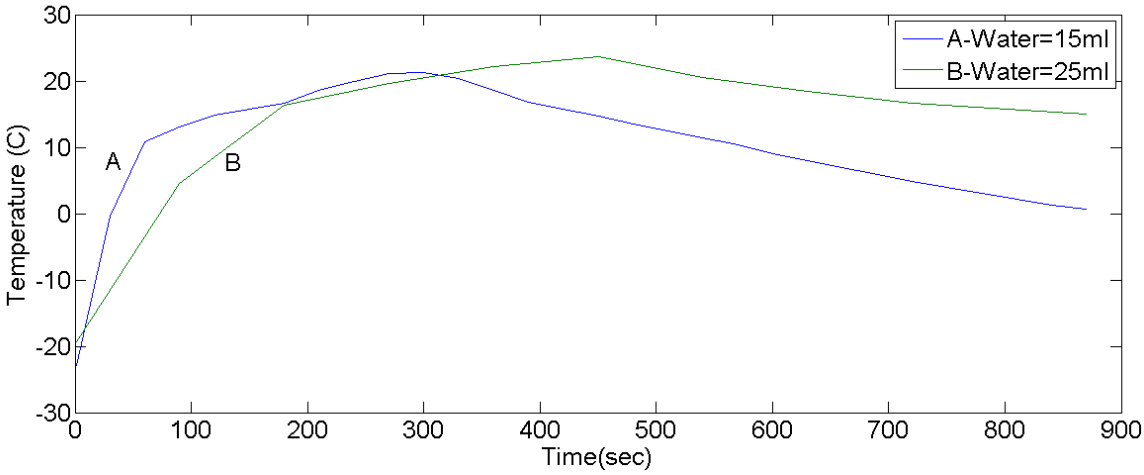

Figure 30- Comparison of temperature profile of 25 gm of Lithium Chloride.

From the graph, it is clear that the energy released by the reaction of B is higher than released in reaction A. This is due to larger quantity of water available for hydration and subsequent crystallization to occur. The temperature rise and fall for experiment A is drastic and for B is relatively gradual. This implies a more sustained release of thermal energy.

5.3 Comparison of Theoretical and Experimental Results

The theoretical model was constructed using nodal analysis and solved using Matlab's ODE 45 function. The theoretical model settles slower than the experimental results. The main reasons for this could be

1. The emissivity of the Aluminum foil is higher than predicted
2. The insulation heat transfer co-efficient is lower than expected.
3. The emissivity of the black interior of the outer sphere is higher than predicted.
4. The battery has lower discharge efficiency than predicted. This would mean lesser internal heat generated.
5. Inaccuracy of the temperature sensor.

The results (Figure 31 and 32) indicate that the predicted thermal inertia and resistance of the system is lower in practice. The internal heat generation and heat transfer co-efficient are primary causes for the deviation. The experimental data is extrapolated as the experiment is performed for 8.25 hours. Steady state temperature is achieved in this time. The theoretical temperature plotted in the graph is the temperature calculated at node zero using the thermal model. The graphs are plotted for a range of specific heat values of abs, the 3d printing material. The maximum value of is 1300 kJ/kgK. The presence of air will reduce the overall specific heat value. The graphs also clearly show that for lower cp values, the temperature profile is almost identical to experimental profile.

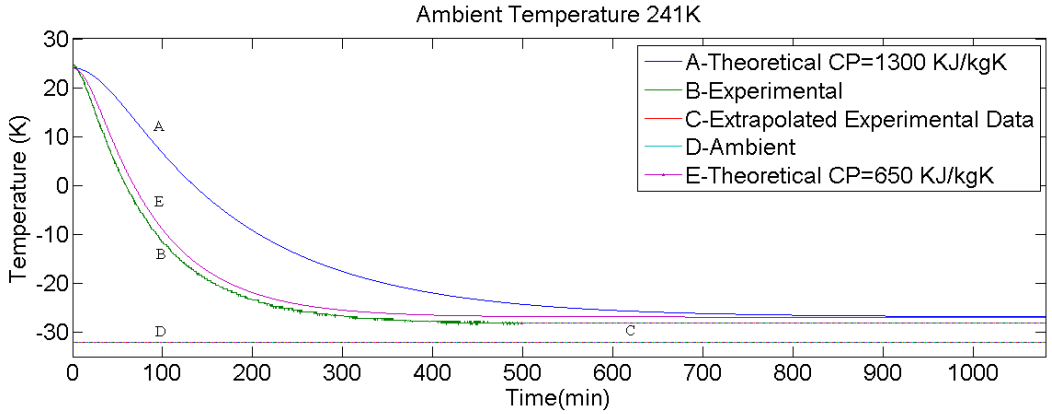

Figure 31- Comparison of temperature profiles of sensor module at -32^{o}C

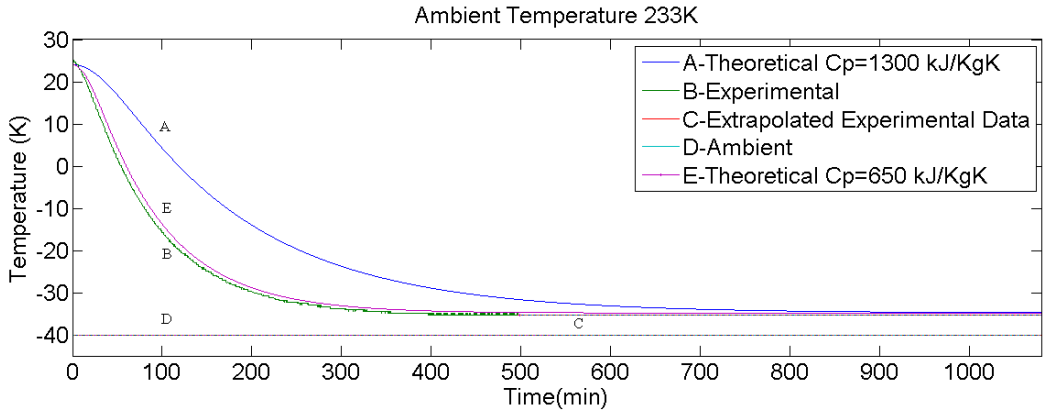

Figure 32- Comparison of temperature profiles of sensor module at -40^{o}C

	Ambient Temperature : -32^{o}C		Ambient Temperature : -40 ^{o}C	
	Theoretical cp=650kJ/KgK	Experimental	Theoretical cp=650kJ/KgK	Experimental
Steady State Temp. (C)	-26.8 ^{o}C	-28.2 ^{o}C	-34.7 ^{o}C	-34.9 ^{o}C
Time(min)	506	383	504	347

Table 12-Theoretical and Experimental Steady State Temperatures

Table 12 shows the variation in the time and temperature between the theoretical and experimental results. The variation in temperature is around 2^{0}C and there is a good agreement in temperature values. The difference in time is very high. This indicates that the experimental thermal inertia is lower than predicted thermal inertia. The time needed to reach steady state experimentally is very similar. The time needed to reach steady state depends on the thermal time constant. The thermal time constant is a function of thermal inertia , internal heat generation and cumulative thermal resistance of the system. All the values are almost equal in both cases, There is a minor difference in the thermal resistances as it is a function of radiative heat loss. Radiation losses depend on the ambient temperatures which are different for both experimental setups.

5.2.1 Comparison of Theoretical performance on Earth and in Space.

The theoretical temperatures in space and on earth are compared below. The temperatures in space will settle at a slower rate and also at a higher temperature. This is due to non-existence of convection losses in space. This reduces the heat loss and as radiation heat transfer is a slow heat transfer mechanism, the rate of temeprature drop is slower. Theoretically, the time required to reach steady state in space is more than twice as on Earth.

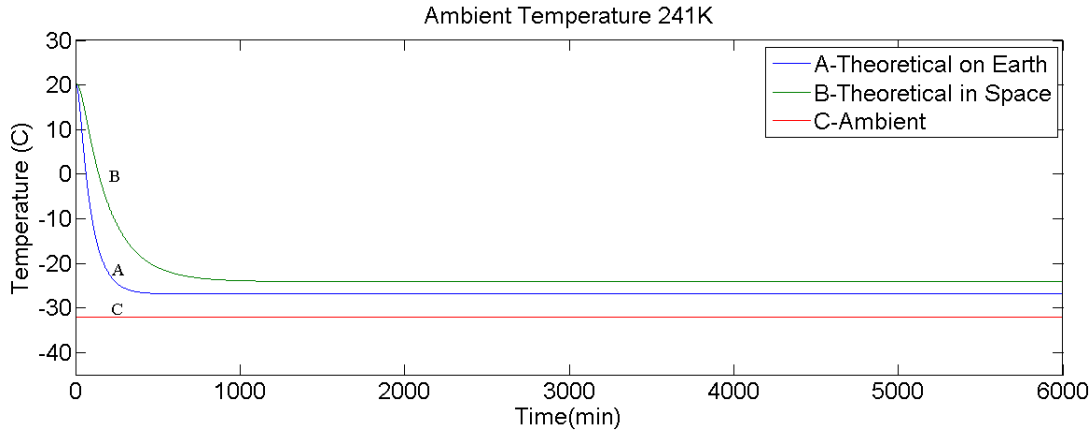

Figure 33 -Comparison of theoretical temperature profiles in space and on Earth at -32^{o}C

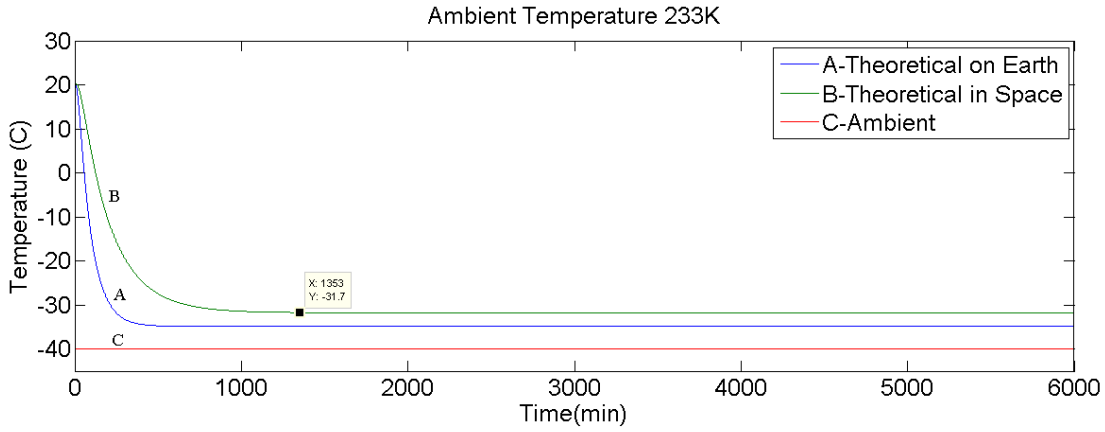

Figure 34 -Comparison of theoretical temperature profiles in space and on Earth at -40^{o}C

	Ambient Temperature : -32^{0}C		Ambient Temperature : -40^{0}C	
	Earth	Space	Earth	Space
Steady State Temperature(C)	-26.8	-24	-34.7	-31.7
Time (min)	506	1107	504	1353

Table 13-Theoretical temperature in space and on Earth

5.4 Experiments at -32°C

The first set of experiments were performed at -32°C. Experiments were performed with three different thermal control systems. They are:

1. Insulation control
2. Heater and insulation control
3. Lithium chloride and insulation control.

The comparison of three systems is done for both sensors in graphs below.

Both sensors have similar temperature profiles with the difference being sensor BMA 250 reaching steady state temperature that is equal to the ambient temperature. The sensor TMP 36 does not reach the ambient temperature. This is due to the least count of the sensor. It is also plausible that as TMP 36 is closer to the SD card, which dissipates more heat in comparison to other on board electronics.

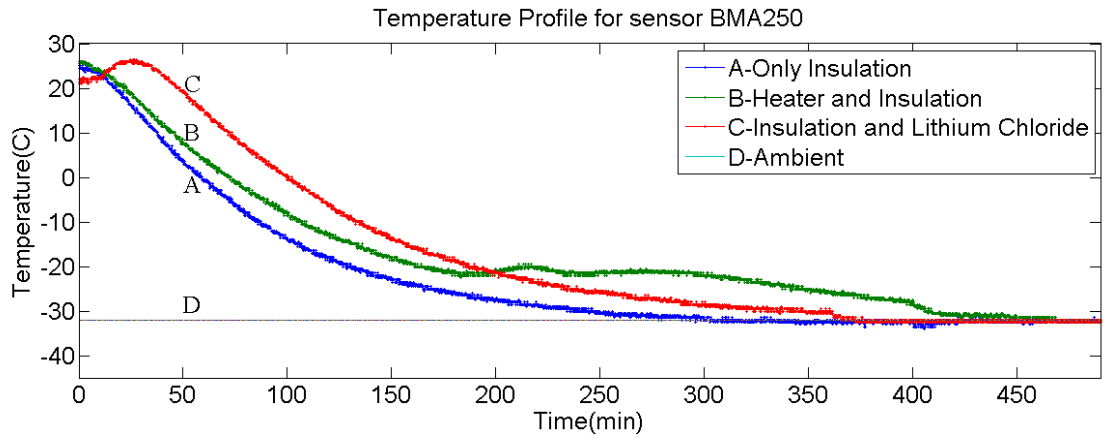

Figure 35-Comparison of experimental temperature profiles at -32^{o}C for sensor BMA250

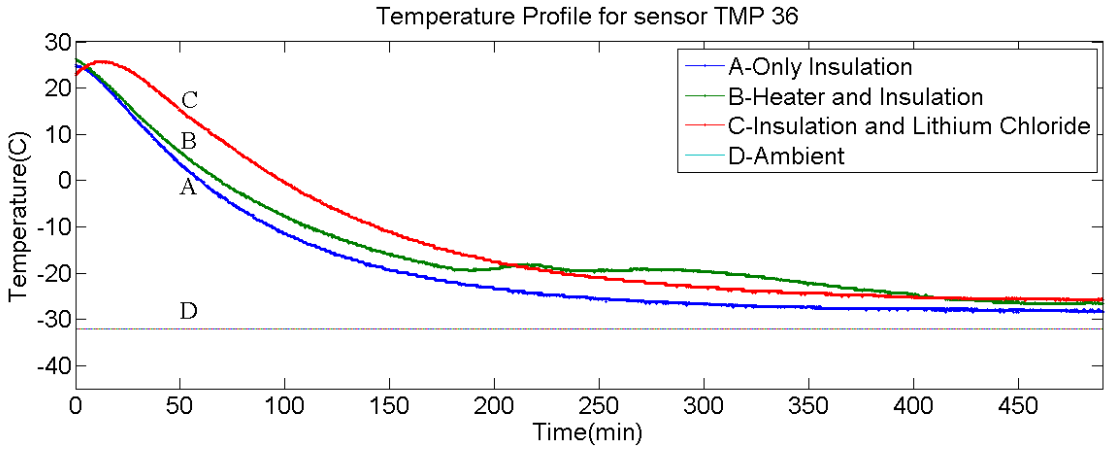

Figure 36- Comparison of experimental temperature profiles at -32^{o}C for sensor TMP 36

In case of the heater profile, it is clear that the PID tries to maintain the temperature at -20 ^{o}C, the desired set point. The heater manages to raise the temperature of the module twice in approximately 100 mins, before the secondary battery can no longer provide the necessary power to raise the temperature. The energy need increases with time as the system continues to drop towards a steady state. As a result, the heat required increases with time to maintain the temperature at -20 ^{o}C.

The thermochemical storage experiment was done with 25gm Lithium chloride and 25ml of water used. The initial heat released causes the temperature to rise by

approximately 5^{o}C for both sensors. The magnitude of temperature rise is not crucial. The temperature profile clearly shows a sustained release of heat, else, the slope of the TCESS profile would drop at a larger rate and merge with the insulation profile. The final settling temperature is almost the same. This difference can be ignored as it is lesser than 2^{0}C which is the maximum error associated with both sensors. The table 13 shows the time needed and the steady state temperatures reached for the different thermal control systems. The following nomenclature is used in the table.

OI-TMP 36 : TMP 36 temperature profile when only insulation is used.

H- TMP 36 : TMP 36 temperature profile when heater and insulation is used.

OI-BMA : BMA 250 temperature profile when only insulation is used.

H- BMA : BMA 250 temperature profile when heater and insulation is used.

Ambient Temperature=241K (-32^{0}C)						
	OI –TMP 36	OI - BMA	H -TMP 36	H -BMA	LiCl TMP 36	LiCl BMA
Steady State Temp(C)	-28.2	-32	-26.36	-32	-25.99	-32
Time(min)	383	315	448	450	412	419

Table 14-Steady state and time data for experiments done at -32^{o}C

5.5 Experiments in ambient -40^{o}C

The experiments were also conducted at -40^{o}C to ensure that the thermochemical performance can be replicated at different ambient temperatures. The graph for both sensors are plotted below.

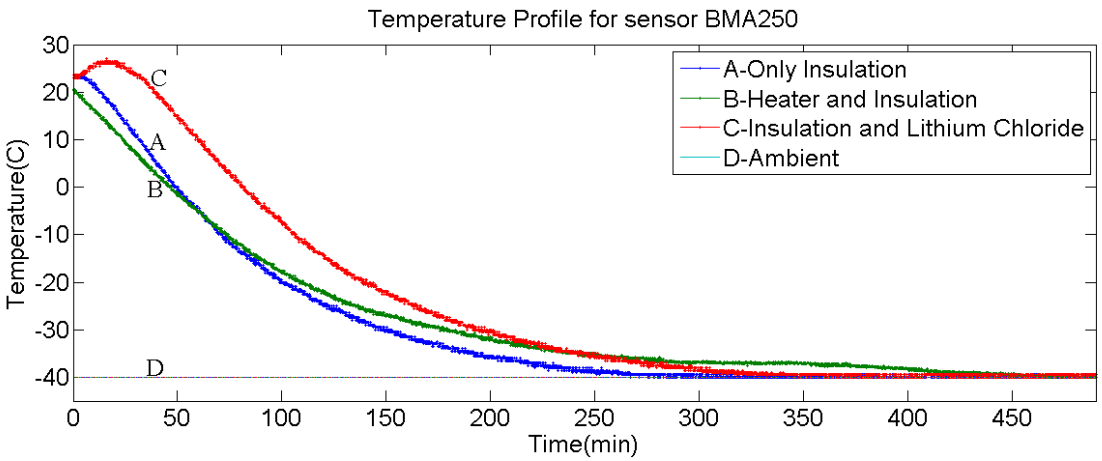

Figure 37- Comparison of experimental temperature profiles at -40^{o}C for sensor BMA250

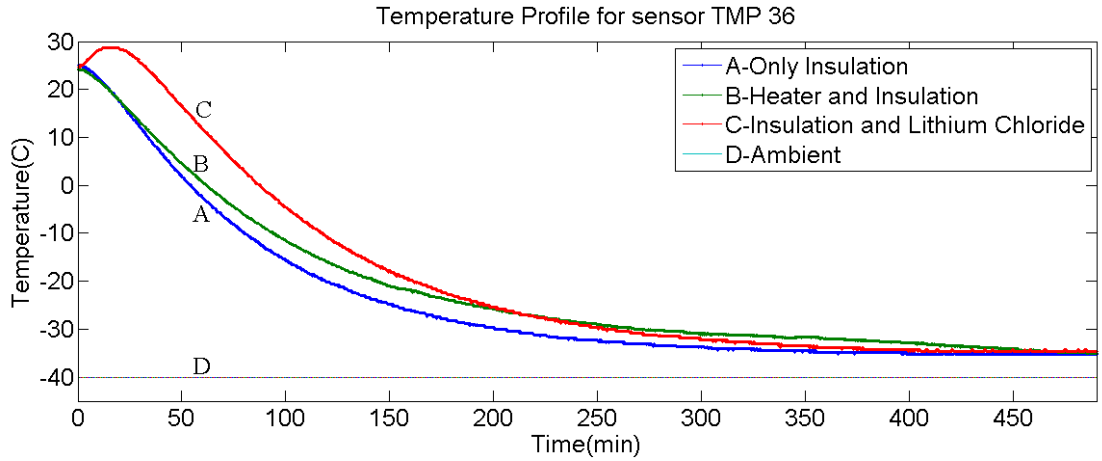

Figure 38- Comparison of experimental temperature profiles at -40^{o}C for sensor TMP36

The profiles are very similar to the experiments conducted at -32^{0}c. As discussed earlier the rate of temperature drop when only insulation is used is very similar to the rate of drop for the -32^{0}C experiment, although the magnitude is different.

The heater profile doesn't show any regulation at -20^{0}C, experimental set point. The heater settles for approximately 100 minutes at -35^{0}C. This indicates although the heater works, it doesn't generate enough power to maintain system at desired set point.

The lithium chloride graph shows an approximately 5^0C rise in temperature before the drop in temperature begins. All three profiles settle at the same temperature but at different times. This proves that this effect can be replicated at different ambient temperatures. Table 14 shows the time needed and the steady state temperatures reached for the different thermal control systems.

Ambient Temperature=233K (-40^{0}C)						
	OI –TMP 36	OI - BMA	H -TMP 36	H -BMA	LiCl TMP 36	LiCl BMA
Steady State Temp(C)	-34.49	-40	-34.38	-40	-34.8	-40
Time(min)	349	280	452	450	365	290

Table 15- Steady state and time data for experiments done at -32^{o}C

The area under the curve is directly proportional to the energy change of the system. This is one way to compare heater and TCESS performance. This magnitude for TCESS is 2362 C.min and for heater is 1349 C.min at -40 ^{o}C. Whereas, for the experiment at -32 ^{o}C these values were found to be 2777 C.min for TCESS and 1901 C.min. Higher values for -32^{o}C proves that both thermal control systems contribute to a larger energy change compared to the experiments at -40^{o}C. This is logical on account of lower heat loss at -32^{0}C. It can hence be concluded that the energy change of the system is likely to be higher in case of TCESS.

5.6 Repeatability Experiments

To verify the performance of Lithium Chloride as salt in TCESS, multiple experiments were repeated and evaluated. The four graphs below show temperature profiles for repeatability experiments conducted at two set ambient temperatures.

Temperatures in figure 39 for experiment three drops below the ambient. Thermodynamically, this is unfeasible. This is clearly due to error in the sensor data acquisition.

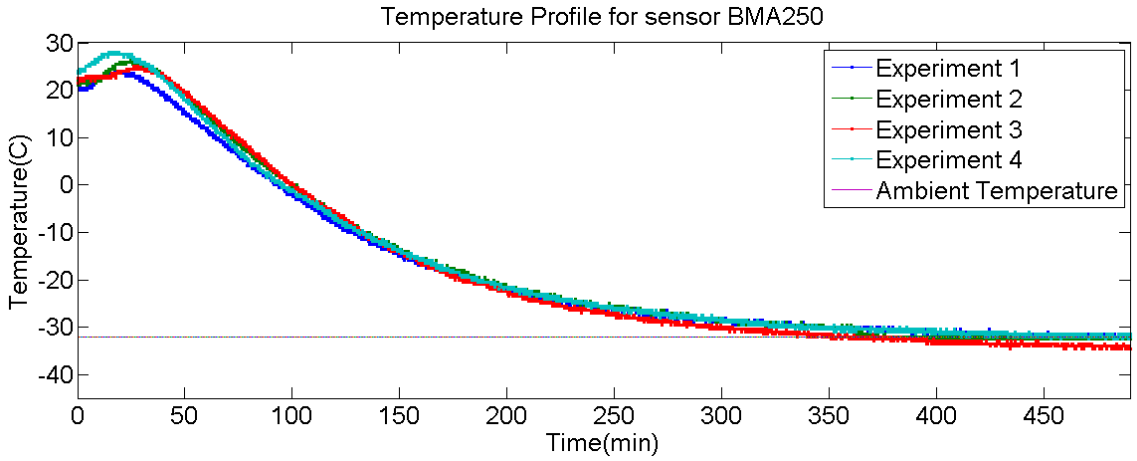

Figure 39-Repeatability experiments at -32^{o}C. Profiles for BMA 250 sensor.

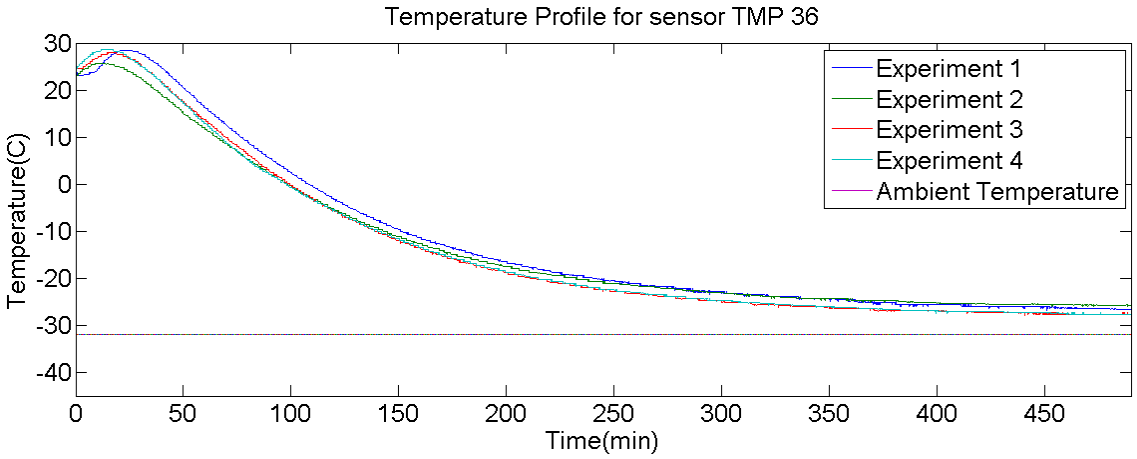

Figure 40- Repeatability experiments at -32^{o}C . Profiles for TMP 36 sensor.

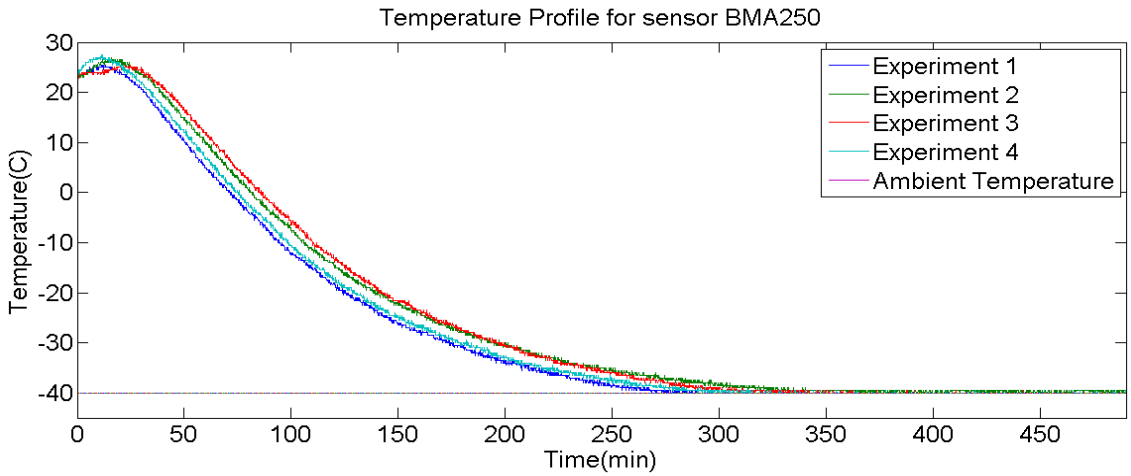

Figure 41- Repeatability experiments at -40^{o}C . Profiles for BMA 250 sensor.

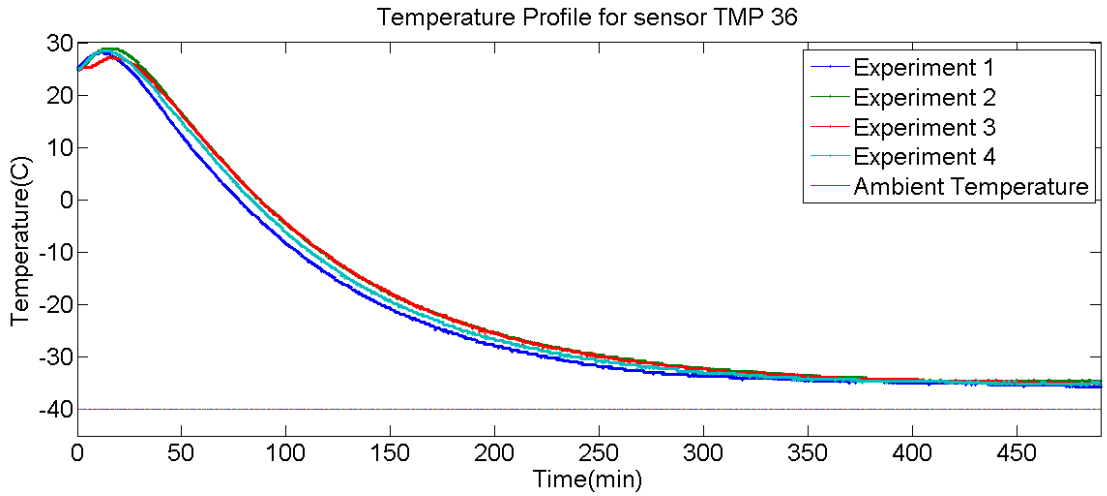

Figure 42- Repeatability experiments at -40^{o}C . Profiles for TMP sensor.

The tables show the time needed and the steady state temperatures reached for the different experiments.

Ambient Temperature=241K (-32^{0}C)								
Experiment run	1		2		3		4	
	LiCl TMP	LiCl BMA	LiCl TMP	LiCl BMA	LiCl TMP	LiCl BMA	LiCl TMP	LiCl BMA
Steady State Temp(C)	-25.99	-32	-25.66	-32	-27.5	-33	-27.08	-32

Time(min)	412	419	422	411	414	411	408	411

Table 16-Repeatability Experiments data for ambient temperature :-32^{o}C

Ambient Temperature=233K (-40^{0}C)								
Experiment run	1		2		3		4	
	LiCl TMP	LiCl BMA	LiCl TMP	LiCl BMA	LiCl TMP	LiCl BMA	LiCl TMP	LiCl BMA
Steady State Temp(C)	-34.8	-40	-34.35	-40	-34.1	-40	-34.6	-40
Time(min)	365	290	380	342	375	300	375	-335

Table 17- Repeatability Experiments data for ambient temperature :-40^{o}C

The main sources of variation in the experiments are:

1. Variation of Refrigerator temperature.

The refrigerator temperature varies ±2^{0}C of the set point. This may cause minor variations in the temperature profile.

2. Quality of Lithium Chloride

The trade study shows that lithium chloride forms different hydrates with different heat of formations and heat of reactions. It should be noted that Lithium Chloride at STP conditions has a DRH of only 11%. If a portion of the salt placed in the container is already hydrated due to minimal exposure to the atmosphere, this may cause the variation.

3. Human Error

The water was sprayed manually on the bed. At this time the external sphere was open. Additionally, time was required to close the module and wrap in aluminum foil. This time variation is small but enough to cause a variation.

5.7 Summary

A thermochemical storage system has been proposed to solve the heating problem

faced by sensor modules in extreme cold temperatures. Using 25 gm of Lithium Chloride, although the improvement in the steady state temperature achieved by the module at -32^0 C and at -40^0C is minimal, there is a measurable increase in the time required to achieve these temperatures. An average increase of 8 % was found at -32^0C and a 9.1 % increase was found at -40 ^{0}C. It should be noted that this increase was achieved using freezing water and not vapor. In case of water, there is a greater chance of a crystalline layer being formed on the surface of the salt bed. It is plausible that this phenomenon reduced further diffusion of water, thus reducing the magnitude of the heat released [17,39]. With water vapor, there should be better diffusion of water molecules through the bed. With proper design it should be possible to improve the performance of the system further.

There is no direct comparison between the performance of the heater and the TCESS. Area under the curve represents only an estimate of the change in energy of the system. The area under the curve for the heater was less than the TCESS for both experiments.

CHAPTER 6

MISSION CONCEPT

The passive thermal control mechanism for sensor modules has been primarily developed for asteroids. The passive thermal heating technology can be used for sensor modules that are designed for use in extreme cold temperature environments . The asteroid Eros has lowest temperatures of -150^{o}C . The rotation period is just above 5 hours. The feasibility of integrating the thermal passives system depends on a number of factors that will influence the final system design. This chapter looks in brief how the work done in this research can be integrated in an actual space systems mission.

A sensor module constellation deployed on the moon can collect valuable scientific data. In the constellation, each node or each sensor module can house different types of sensors.

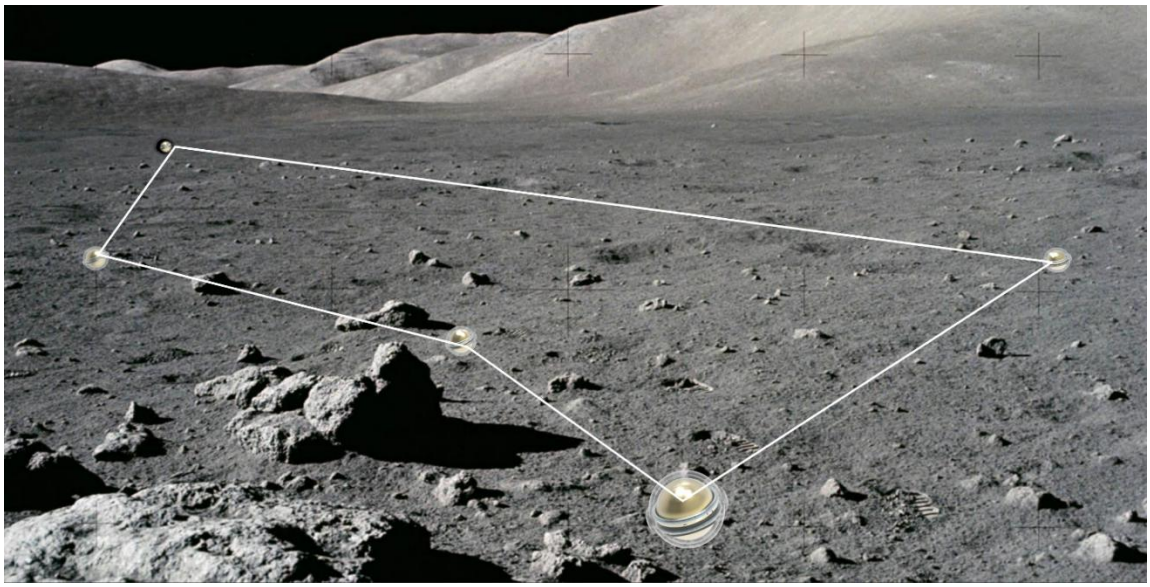

Figure 43- Sensor Module Network

The recharging of the system will take place once the module is exposed to sunlight. It is preferable to have the thermochemical storage system attached to the inner sphere. In this case the outer sphere can be made of a coating that changes it absorptive properties based on the external environment. The thermochemical storage can also be attached to the external sphere, however in this case the heating effect on the inner sphere will be diminished. If the electronics dissipate higher quantity of heat during day time operations, this heat can also be used to assist in regeneration. The aim of the thermochemical storage system will be to reduce the rate of the temperature drop. The temperature profiles on Eros with different thermal control systems are compared below.

In a space rated design, it is necessary to have the lithium chloride layer on the external sphere rather than on the internal sphere. This is will ensure regeneration can take place. The lithium chloride can be used in the form of sponges similar to the design employed by SEAR.

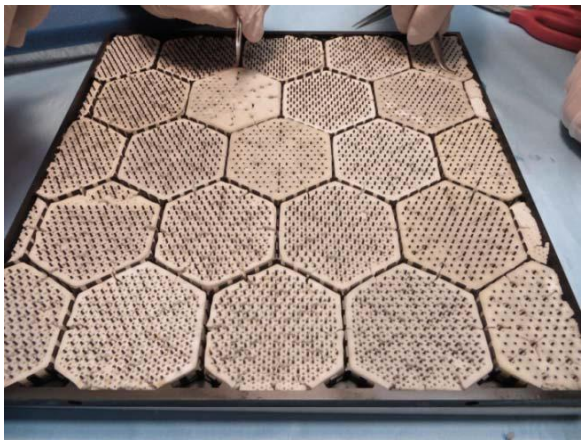

Figure 44-Lithium chloride sponges[21]

As the heating effect is not produced adjoining the internal sphere, the heat needed will be larger. This will directly increase the quantity of water vapor and lithium chloride needed.

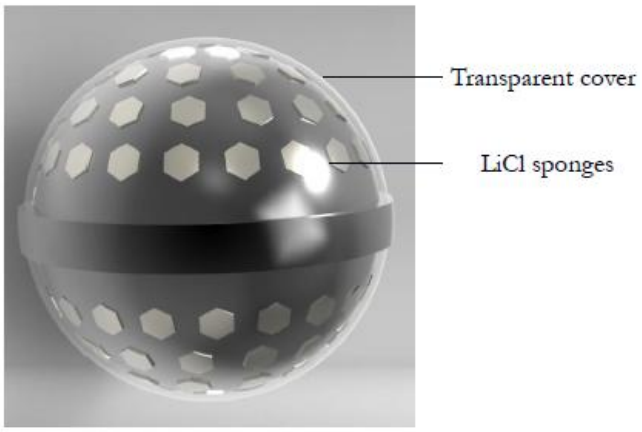

Figure 45-Mission concept outer sphere design

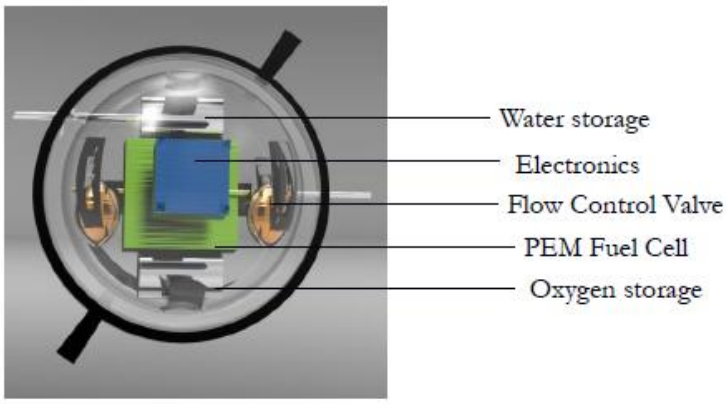

Figure 46-Mission concept inner sphere design.

The main sub systems of the sensor module are explained below :

6.1 Instruments

Various miniaturized instruments can be used to collect different data. Some of the sensors are explained below.

6.1.1 Camera

The gumstix tiny caspa camera has a form factor of 22mm x 22mm and operates at 3.3 V. This power requirement is similar to the Tinyduino Processor.

Figure 47- Gumstix Camera[41]

6.1.2 Inertial Measurement Unit (IMU)

IMU's are used to measure accelerometer and angular velocity data. IMU's like tinyduino's 9-axis IMU also have a 3d digital magnetic sensor, giving it capabilities to detect magnetic anomalies. The moon for example, is rife with magnetic anomalies. A 3-axis magnetic field will provide more accurate information of these anomalies than existing topological and geological maps. [42]

6.2 Thermal Sub System

6.2.1 Thermal System Block Diagram

In a conventional thermal space system , the heating effect is provided by Kapton Heaters. Kapton heaters are used to heat critical subsystems rather than provide heating to the entire spacecraft. The block diagram for the conventional system is drawn below.

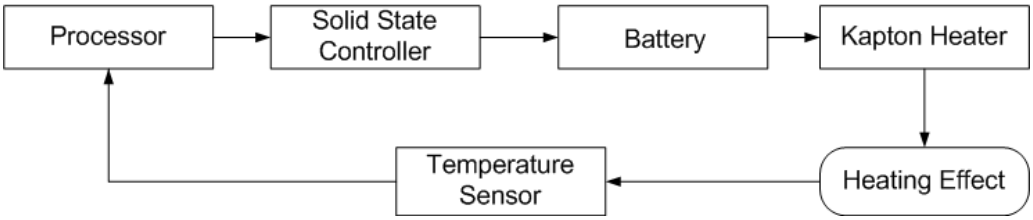

Figure 48- Conventional thermal system block diagram

The feasibility of a passive thermal control system depends highly controlling the reaction rate. They showed that although the hydration reaction will generate heat , there is only a minor increase in the time taken to reach steady state. The literature survey has shown that the heat released will increase if the flow rate of the sorbate is controlled. This mechanism will hence control the rate of heat production. The block diagram for this system is shown below. The system will have a flow control valve and a micro pump. Similar to the conventional system, a processor will check the temperature sensor data. In this system, temperature sensor will actuate the flow control valve. The water vapor flow onto the dehydrated salt bed will give the necessary heating effect. Once the set point is reached, the processor will stop the flow control valve.

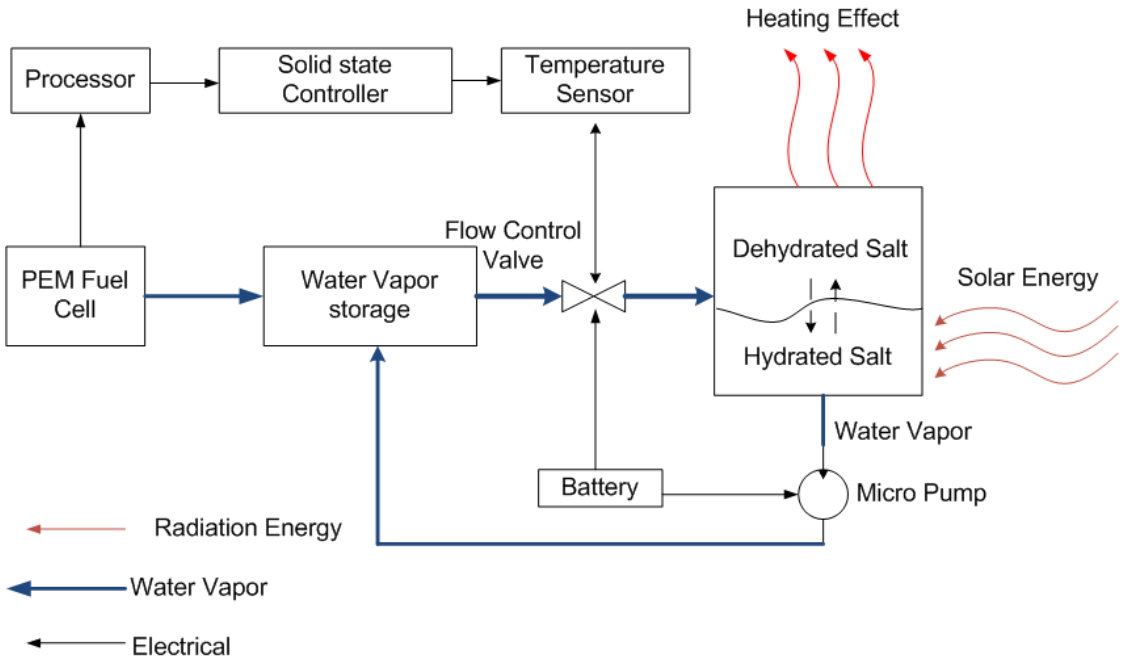

Figure 49- Thermochemical storage system block diagram

The temperature profiles are predicted on Asteroid Eros. Eros has an approximate rotation period of 315 minutes. There will be parts of Eros shrouded in darkness for this entire duration. The TCESS can ensure survival in such conditions. The thermal model used to select the optimum geometry of the sensor module is used to predict the difference. Approximately 2W of power needs to be generated on the external surface of the outer sphere. Over a period of 5 hrs, this 10Whr of heat energy. From the trade study it is clear that the lithium chloride required would be less than 30gm assuming less than 50% efficiency in heat production. A performance increase of 90% can be achieved using this system.

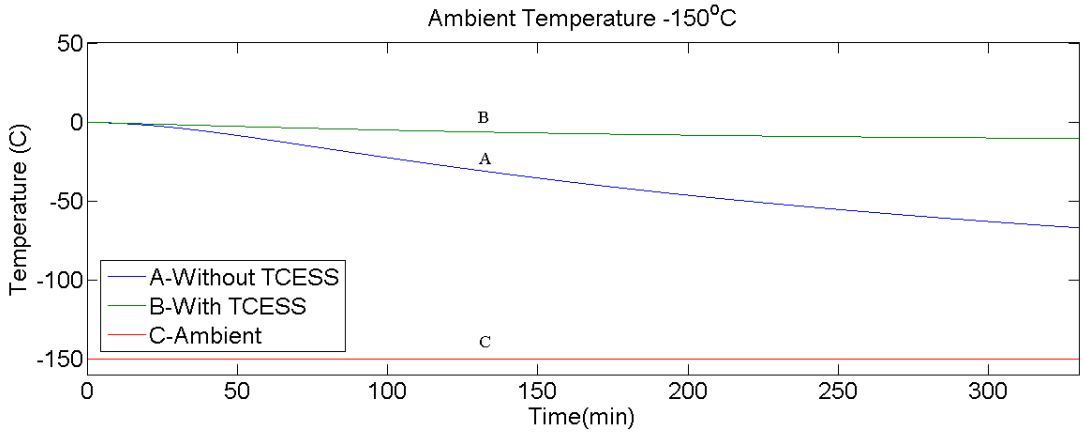

Figure 50-Comparsion of temperatures on Eros

6.2.2 Flow Control Valve

It is necessary to have a micro electronic flow control valve for this purpose. The flow control valve coupled with a pressure regulator manufactured by SSC Nanospace can be used for propellants such as xenon and steam. In vacuum , due to very low vapor pressure, the water from a fuel cell should immediately convert to water vapor. This means the flow control valve is a viable option. A micro pump will be needed to flow the vapor back to the water vapor storage tank upon dehydration of the salt.

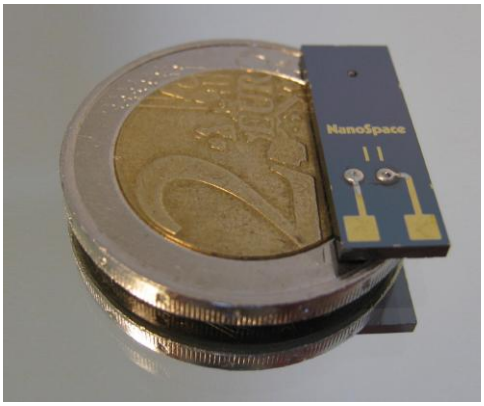

Figure 51- Flow Control valve [42]

6.2.3 Thermo chemical storage material

The thermochemical storage material will be used to produce an exothermic reaction to provide heat to the sensor module. The thermochemical material can be chosen depending on the magnitude of the heating effect that needs to be provided.

6.2.4 Multi layer insulation and surface coatings

MLI is used to reduce the rate of the heat loss of a system Aluminized Kapton and Aerogel are viable options. Optical properties can be varied using various surface coatings.

6.3 Mass Budget

The system mass budget is described below. The change in mass is on account of using Aluminum Chassis rather than a 3D printed chassis.

Subsystem	Component	Mass(g)	Max. Deviation	Max. Mass(g)
Structure	Outer sphere	480	1.2	576
	Inner Sphere	270	1.2	324
	Connector ring	15	1.1	16.5
	TCM container	21	1.1	23
	Water Tank	20	1.5	30
	Oxygen Tank	20	1.5	30
Command & data Handling	Tinyduino Processor	4	1.1	4.4
	SD card module	4	1.1	4.4
Communication	Tinyduino comms. board	7	1.1	7.7
Sensors	Camera	10	1.1	11
	TMP 36	2	1.1	2.2
Power	PEM Fuel Cell	15	1.3	19.5
	Lithium Hydride	25	1.5	37.5

	Water Vapor	25	1.1	27.5
Thermal	Insulation	3	1.1	3.3
	TCM salt	25	1.2	30
	Flow control valve	20	1.5	30
	micro pump	20	1.5	30
Miscellaneous	Nuts	5	1.2	6
	bolts	5	1.2	6
	Tubing	30	1.5	45
Total		1026		1265

Table 18-Mass Budget

6.4 Power Budget

Subssystem	Component	Power generated(mW)	Margin	Max. Power(W)
Command & data handling	Processor	4.2	1.2	0.0050
	SD Card	350	1.2	0.42
Sensors	Sensor board	0.49	1.1	0.00053
	TMP 36	0.17	1.1	0.00019
Instrument	Camera	500	1.5	0.75
Communication	Radio (Receiving)	55	1.2	0.066
	Radio (Transmitting)	90	1.2	0.108
Miscellaneous	Flow control Valve	100	1.5	0.15
				1.5

Table 19-Power Budget

CHAPTER 7

CONCLUSION

7.1 Conclusion

- A spherical configuration for a wireless sensor module has been designed and 3D printed.
- The thermal modeling of the sensor module for both space and earth applications has been done.
- A heating effect produced by the hydration reaction of Lithium Chloride and water at sub-zero temperatures has been demonstrated at lab scale.
- Performance of sensor module with different thermal architectures is done at -32^0C and -40^0C. The steady state temperature remains approximately same but Lithium chloride based design provides increase in time required to achieve steady state. An average increase of 9% at -40^0C and 8.1% at -32^oC found using TCESS.
- Repeatability experiments done with Lithium Chloride show the heating effect can be reproduced.
- The TCESS is predicted to produce an 80% performance enhancement on Asteroid Eros

7.2 Future Work

- Development of composite materials to improve thermochemical storage system
- Experiments to be done in Vacuum environment.
- Determine experimentally effect of flow rate of sorbate on the produced heating effect.

- Develop a rechargeable thermochemical storage system.

References

[1]."ESA Science & Technology: Philae Lander." Accessed October 21, 2016. http://sci.esa.int/rosetta/53297-philae-lander/.

[2]."Hopping 'Hedgehog' Robot Could Explore Comets and ..." Accessed October 21, 2016. http://www.space.com/30487-nasa-hedgehog-robot-space-exploration.html.

[3]."Fuel Cell Store." Accessed October 21, 2016. http://www.fuelcellstore.com/.

[4].D. Strawser, J. Thangavelautham, S. Dubowsky 'Feasibility Study of Long-Life Micro Fuel Cell Power Supply for Sensor Networks for Space and Terrestrial Application.', Hydrogen Energy 39 (2014) pp 10216-10229, Solid State Ionics

[5].Kavya Kamal Manyapu 'Feasibility Study of Long-Life Micro Fuel Cell Power Supply for Sensor Networks for Space and Terrestrial Applications ', 2010. Master's Thesis in Aeronautics and Astronautics, MIT

[6].Strawser, D., J. Thangavelautham, and S. Dubowsky. 2014. A passive lithium hydride based hydrogen generator for low power fuel cells for long-duration sensor networks. International Journal of Hydrogen Energy 39 (19): 10216-29.

[7]."Fuel Cell Basics — Fuel Cell & Hydrogen Energy Association." Accessed October 21, 2016. http://www.fchea.org/fuelcells/.

[8].Morin, A., Z. Peng, J. Jestin, M. Detrez, and G. Gebel. 2013. Water management in proton exchange membrane fuel cell at sub-zero temperatures: An in operando SANS-EIS coupled study. Solid State Ionics 252 : 56-61.

[9].Larson, Wiley J., James Richard. Wertz, and Brian D'Souza. SMAD III: Space Mission Analysis and Design, 3rd Edition: Workbook. El Segundo, CA.: Microcosm Press, 2005., 512-534

[10]. Gilmore, David G. Spacecraft Thermal Control Handbook. El Segundo, CA: Aerospace Press, 2002.

[11]. Kapton® Plays Important Role on Rosetta Mission." Accessed October 21, 2016. http://www.dupont.com/products-and-services/membranes-films/polyimide-films /kapton-polyimide-film

[12]. "Www.accuglassproducts.com." Accessed October 21, 2016. http://www.accuglassproducts.com/home

[13]. "Cryocoolers for Space Applications — Cryogenic Engineering ..." Accessed October 21, 2016. http://www.eng.ox.ac.uk/cryogenics/research/cryocoolers-for-space-applications.

[14]. Dipl.-Phys.Armand Fopah Lele ,'2015. A Thermochemical Heat Storage System for Households: Thermal Transfers Coupled to Chemical Reaction Investigations', 'PHD dissertation Unversitat Luneburg

[15]. Wu, Juan, and Xin feng Long. 2015. Research progress of solar thermochemical energy storage: Thermochemical energy storage of solar energy. International Journal of Energy Research 39 (7): 869-88.

[16]. Ding, Yate, and S.b. Riffat. "Thermochemical Energy Storage Technologies for Building Applications: A State-of-the-art Review." Int. J. Low-Carbon Tech. International Journal of Low-Carbon Technologies 8, no. 2 (2012): 106-16. doi:10.1093/ijlct/cts004.

[17]. Yu, N., RZ Wang, and LW Wang. 2013. Sorption thermal storage for solar energy. Progress in Energy and Combustion Science 39 (5): 489-514.

[18]. P. Gantenbein, S. Brunold, F. Flückiger, U. Frei, sorbtion materials for application in solar heat energy storage

[19]. Abedin, Ali Haji. "Energy and Exergy Analyses of an Open Thermochemical Energy Storage System: Methodology and Illustrative Application." The Open Renewable Energy Journal TOREJ 5, no. 1 (2012): 41-48. doi:10.2174/1876387101205010041.

[20]. Tatsidjodoung, Parfait, Nolwenn Le Pierrès, and Lingai Luo. 2013. A review of potential materials for thermal energy storage in building applications. Renewable and Sustainable Energy Reviews 18 : 327-49.

[21]. Michael G. Izenson, Weibo Chen, Scott Phillips, Ariane Chepko 'High-Capacity Spacesuit Evaporator Absorber Radiator(SEAR)' 45th International Conference on Environmental Systems ICES-201512-16 July 2015, Bellevue, Washington.

[22]. Nonnen, Thomas, Steffen Beckert, Kristin Gleichmann, Alfons Brandt, Baldur Unger, Henner Kerskes, Barbara Mette, et al. 2016. 'A thermochemical long-term heat storage system based on a Salt/Zeolite composite'. Chemical Engineering & Technology.

[23]. Liu, Hongzhi Nagano, Katsunori Togawa, Junya 'A composite material made of mesoporous siliceous shale impregnated with lithium chloride for an open sorption thermal energy storage system', Solar Energy; 111; 186-200; Solar Energy.

[24]. Yu, N., L. W. Wang, R. Z. Wang, and Z. S. Lu. 2015. Study on consolidated composite sorbents impregnated with LiCl for thermal energy storage. International Journal of Heat and Mass Transfer 84 : 660-70.

[25]. N'Tsoukpoe, KE, T. Schmidt, HU Rammelberg, BA Watts, and WKL Ruck. 2014. A systematic multi-step screening of numerous salt hydrates for low temperature thermochemical energy storage. Applied Energy 124 : 1-16.

[26]. "All Products - TinyCircuits." Accessed October 21, 2016. https://tinycircuits.com/collections/all

[27]. "TMP36 Datasheet and Product Info | Analog Devices." Accessed October 21, 2016. http://www.analog.com/en/products/analog-to-digital-converters/integrated-special-purpose-converters/integrated-temperature-sensors/tmp36.html.

[28]. "Dual Motor TinyShield - TinyCircuits." Accessed October 21, 2016. https://tinycircuits.com/products/dual-motor-tinyshield.

[29]. Larminie, James, and Andrew Dicks. 2000. Fuel cell systems explained. New York;Chichester [England]; Wiley. 399-400

[30]. BuyAerogel.com | Thermal Wrap™ 6-mm Blanket." Accessed October 21, 2016. http://www.buyaerogel.com/product/thermal-wrap/.

[31]. Laguerre, O., S. Ben Amara, J. Moureh, and D. Flick. 2007. Numerical simulation of air flow and heat transfer in domestic refrigerators. Journal of Food Engineering 81 (1): 144-56.

[32]. Yunus A. Cengel Afshin J Ghajar , Heat and Mass Transfer, 543-544

[33]. ABS Heat Resistant | Commodity Polymers - Matbase.com." Accessed October 21, 2016.www.matbase.com/material-categories/natural-and-synthetic-polymers/commodity-polymers/material-properties-of-acrylonitrile-butadiene-styrene-heat-resistant-abs-heat-resistant.

[34]. Paksoy, Halime Ö., 2007; Thermal energy storage for sustainable energy consumption: Fundamentals, case studies and design. Vol. 234. Dordrecht: Springer, 393

[35]. De Jong, Ard-Jan, Fanny Trausel, Christian Finck, Laurens Van Vliet, and Ruud Cuypers. 2014. Thermochemical heat storage - system design issues.

[36]. Monnin, Christophe, Michel Dubois, Nicolas Papaiconomou, and Jean-Pierre Simonin. 2002. Thermodynamics of the LiCl + H2O system. Journal of Chemical and Engineering Data 47 (6): 1331-6

[37]. N'Tsoukpoe, K. Edem, Hui Liu, Nolwenn Le Pierrès, and Lingai Luo. 2009. A review on long-term sorption solar energy storage. Renewable and Sustainable Energy Reviews 13 (9): 2385-96.

[38]. Yan, T., R. Z. Wang, L. W. Wang, T. X. Li, and Ishugah T. Fred. 2015. A review of promising candidate reactions for chemical heat storage. Renewable and Sustainable Energy Reviews43 : 13-31.

[39]. Trausel, Fanny, Ard-Jan De Jong, and Ruud Cuypers. 2014. A review on the properties of salt hydrates for thermochemical storage.

[40]. Tsunakawa, H., F. Takahashi, H. Shimizu, H. Shibuya, and M. Matsushima. 2014. Regional mapping of the lunar magnetic anomalies at the surface: Method and its application to strong and weak magnetic anomaly regions. Icarus 228 : 35-53.

[41]. "Tiny Caspa 0.3MP 27-pin Camera Board." Tiny Caspa 03mp 27-pin Camera Board. Accessed October 27, 2016. https://store.gumstix.com/cameras-displays-gps/tiny-caspa

[42]. "Micropropulsion NanoSpace SSC." Accessed October 21, 2016. http://www.sscspace.com/Products-Services/space-propulsion-1/nanospace-7/micropropulsion.